A

Dissertation

on

Development of new flowsheet for the synthesis of nano zirconium carbide (ZrC)

Submitted in the partial fulfilment of the requirements for award of degree of

Master of Science

in

Physics

(2015-2017)

submitted by

Amit Singh Vig

(301504003)

under the guidance of

Dr. O. P. Pandey

(Senior Professor)

SCHOOL OF PHYSICS AND MATERIALS SCIENCE,

THAPAR UNIVERSITY

PATIALA (PUNJAB)-147004

July, 2017

CERTIFICATE

This is to certify that this dissertation entitled **Development of new flowsheet for the synthesis of nano zirconium carbide (ZrC)** which is being submitted by ***Mr. Amit Singh Vig (301504003)*** in fulfilment of the requirements for the award of the degree of Master of Science in Physics from School of Physics and Materials Science, Thapar University, Patiala, (Punjab), India. It is an exclusive record of candidate's own research work under the supervision of ***Dr. O. P. Pandey***. The dissertation in part or in full has not been submitted in any other university or institute for the award of any degree.

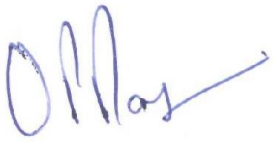

Dr. O. P. Pandey

(Supervisor)

Senior Professor

School of Physics and Materials Science

Thapar University, Patiala

ACKNOWLEDGEMENT

After an extensive period of six months, I take this opportunity to write this note as a final touch of dissertation to express my gratitude and acknowledge the individuals who have been there for me in the completion of my thesis. These past few months were intense for me not only in the scientific but also on a personal level. The realm of time has taught me a lot and this dissertation has had a big impact on me. I would like to commence by thanking the people who helped me throughout this period.

Prima face, I would like to thank my mentor and guide **Dr. O. P. Pandey** (Senior Professor, School of Physics and Materials Science) for his valuable guidance and constant support throughout the course of this work. He is the one who envisioned this project and deemed me worthy of doing this work. I thank him for his constructive criticism and the patience he has shown towards me. I would also like to thank **Mr. Aayush Gupta** for embarking on this journey with me and staying with me till the end, no matter how I felt, he was there for me throughout. Whenever I got stuck somewhere he is the one who helped me pull out of the situation and with such ease. He has been a friend, an elder brother and my co-mentor who believed in me more than I believed in myself and I thank him from all my heart.

It is my privilege to thank **Prof. Prakash Gopalan**, Director, Thapar University, Patiala, for providing the resources for my research work.

I would also like to thank Dr. B. N. Chudasama, Dr. Loveleen Kaur Brar, Dr. Manoj Sharma (Head SPMS) for their valuable support and help throughout the dissertation.

I would also like to thank **Mr. Indermani Mishra**, **Mrs. Neelam Sadana, Mr. Purshottam Singh, Mr. Jant Singh** and **Mr. Pardeep Singla** for helping me at various times. I would like to extend my thanks to **Mr. Ghanshyam Morya** and **Mr. Mukesh Aggarwal** at SAI labs for their help.

My lab mates at functional materials lab, were my constant source of encouragement and so I would also like to thank them, **Ms. Harneet Kaur**, **Dr. Gurbinder Kaur**, **Mr. Rameez Mir**, **Mr. Piyush Sharma, Mr. Varun Singhal**, **and Ms. Taranpreet Kaur**. Thank you for being there in all the ups and downs, for all the toffees and parties we had together.

I find this an opportune time to thank all my friends from whom I have gained a lot. It is because of them that I have learned how to be strong, firm and take a stand for myself.

I want to express my love for the two people in my life for whom the words fell short when I thank them, my sweet and the world's best parents **Mr. Tajinder Singh** and **Mrs. Satnam Kaur.** Never have they ever stopped me in doing anything in my life and have cascaded their love on me continuously and it is because of their constant support and encouragement which have got me where I am today, I thank them for showing me the path in achieving my goals. A short and sweet thanks to my sister **Komalpreet** and my sweet pet **Ozzy**, whenever I was down seeing him play would made my day.

And above all, to the almighty **Waheguru**, for always providing me with the best and showering his blessing upon me.

Amit Singh Vig

ABSTRACT

Scientist for the past two centuries have been fascinated by carbides due to their unique physical, chemical and mechanical properties. It is because of their high melting point that they form refractory carbides and falls in the category of ultra high temperature ceramics (UHTC). Their hardness is also very high due to which they find use in production of drill bits and cutting tools. Among these carbides, ZrC is a very significant compound due to its distinctive features and thus is useful for industrial applications. Keeping this in mind, ZrC nanopowders were synthesized in the present study via a carbothermal-reduction technique by using ZrO_2 as a precursor for Zr and C_6H_{14} as a C source along with Mg as a reductant. Various experiments were performed by varying temperature (600, 700, and 800 °C), holding time (2.5 and 7.5h), and in the later stages varying the C content to observe the changes in the morphology of the compound. All the synthesis was done in a sealed stainless steel autoclave in a furnace at a heating rate of 5 °C/min. Synthesized samples were characterized by X-ray diffraction, scanning electron microscope and transmission electron microscope. The thermal analysis was done using thermal gravimetric analysis/ differential scanning calorimetry. XRD results illustrated that heating the precursors at 700 °C with a holding time of 10h is optimum condition to produce single phase ZrC. The nanoparticles produced have an average size of about 26 nm having a C layer engulfed structure. The factors influencing the synthesis of ZrC have been discussed in the present work.

List of Figures

	Page
1.1 Categorization of carbides based on bond nature.	2
1.2 Crystal structure of FCC TMCs.	5
1.3 Comparison of melting points of TMs and TMCs.	6
1.4 Comparison of densities of TMs and TMCs.	6
1.5 Phase diagram of Zr-C system.	10
3.1 Methodology for synthesizing and characterizing nano zirconium carbide (ZrC).	27
4.1 Effect of synthesis temperature on the developed phases during the formation of ZrC.	32
4.2 Effect of holding time at 800 °C on the synthesis of ZrC.	33
4.3 Variation of lattice parameter at different holding time at 800 °C.	34
4.4 Variation of carbon content at 5h holding at 800 °C.	35
4.5 Variation of lattice parameter with varying carbon content at 800 °C.	36
4.6 The W-H analysis of the sample '5ZrC700', the crystalline size is extracted from the y-intercept of the fit. The strain and stress is extracted from the slope (a) Pearson VII fitted data, (b) USM.	37
4.7 The W-H analysis of the sample '10ZrC700', the crystalline size is extracted from the y-intercept of the fit. The strain and stress is extracted from the slope (a) Pearson VII fitted data, (b) USM.	37
4.8 The W-H analysis of the sample '5ZrC800', the crystalline size is extracted from the y-intercept of the fit. The strain and stress is extracted from the slope (a) Pearson VII fitted data, (b) USM.	38
4.9 The W-H analysis of the sample '10ZrC800', the crystalline size is extracted	38

from the y-intercept of the fit. The strain and stress is extracted from the slope (a) Pearson VII fitted data, (b) USM.

4.10 The W-H analysis of the sample '2.5ZrC800', the crystalline size is extracted from the y-intercept of the fit. The strain and stress is extracted from the slope (a) Pearson VII fitted data, (b) USM. 39

4.11 The W-H analysis of the sample '5ZrC800 C0.22', the crystalline size is extracted from the y-intercept of the fit. The strain and stress is extracted from the slope (a) Pearson VII fitted data, (b) USM. 39

4.12 DSC/TGA study of (a) 5ZrC700 and (b) 5ZrC800 C0.22. 42

4.13 (a) HRTEM micrograph showing morphological features of sample 5ZrC700, (b) HRTEM micrograph of 5ZrC800 C0.22 having agglomerated morphology. 43

4.14 (a) HRTEM micrograph of sample 5ZrC700 indicating the carbon layer on ZrC particle, (b) lattice fringes of plane (200) of cubic ZrC. 44

4.15 (a) HRTEM micrograph of sample 5ZrC800 C0.22 indicating the carbon layer on ZrC particle, (b) lattice fringes of plane (111) of cubic ZrC. 44

4.16 SAED pattern micrograph of sample (a) 5ZrC700 (b) 5ZrC800 C0.22 of cubic ZrC 45

4.17 (a) Absorption spectra of sample 5ZrC700 in the range 300-650 nm, (b) Tauc plot of 5ZrC700 with band gaps of 2.22 eV and 2.66 eV. 46

4.18 (a) Absorption spectra of sample 5ZrC800 C0.22 in the range 300-650 nm, (b) Tauc plot of 5ZrC800 C0.22 with band gaps of 2.55 eV and 2.82 eV. 46

4.19 (a) Absorption spectra of MB dye at various exposure intervals, (b) %age degradation of 5ZrC800 C0.22 at different intervals of time. 48

List of Tables Page

1.1 Crystal structure of transition metal (M) and their carbides (MC). 4

1.2 Comparison data of the TMCs of group IV, V and VI. 8

1.3 Reaction of ZrC with metals and metal oxides. 9

3.1 Data of the experimental conditions for preparing ZrC nano powders. 27

4.1 List of standard ICDD cards used in proposed work. 31

4.2 Williamson – Hall analysis of each of the synthesized samples. 40

4.3 List of d-spacing and lattice constants of synthesized samples. 41

Table of contents

S.No.	Page
Certificate	i
Acknowledgement	ii
Abstract	iv
List of Figures	v
List of tables	vii

Chapter – 1

1-15

1. Introduction	1
1.1 Transition metal carbides (TMCs)	1
1.2 Application of TMCs	2
1.3 Crystal structure and compostion	3
1.4 Physical properties of TMCs	5
1.4.1 Melting point	5
1.4.2 Density	6
1.5 Resistivity	7
1.6 Mechanical properties	7
1.7 Chemical properties	7
1.8 Zirconium – carbon (Zr-C) system	9
1.9 Phase relationship of ZrC system	10
1.10 Properties of zirconium carbide	10
1.10.1 Lattice parameter and density	10
1.10.2 Chemical reactivity	11
1.10.3 Heat of formation	11
1.11 Advantages of zirconium carbide over other TMCs	11
1.12 References	13

Chapter – 2

16-25

2. Literature review 16

2.1 References 23

Chapter – 3

26-30

3. Experimental work 26

3.1 Methodology 26

3.2 Characterizations 28

3.2.1 X-ray diffraction (XRD) 28

3.2.2 Differential scanning calorimetry/Thermal gravimetric analysis 28

3.2.3 High resolution transmission electron microscopy (HRTEM) 28

3.2.4 UV-Vis spectroscopy 29

3.2.5 Photocatalytic activity 29

3.3 References 30

Chapter – 4

31-50

4. Results and discussion 31

4.1 X-ray diffraction (XRD) analysis 31

4.1.1 Effect of temperature on the synthesis of ZrC 31

4.1.2 Effect of variation of holding time at 800 °C on the synthesis of ZrC 33

4.1.3 Effect of variation of carbon content at 800 °C on the synthesis of ZrC 34

4.2 Williamson – Hall analysis 36

4.3 Thermal analysis 42

4.4 Microstructural analysis 43

4.5 Optical analysis 46

4.6 Photocatalytic activity 47

4.7 References 49

Chapter – 5

5. Conclusion 51

Chapter – 6

6. Future Scope 52

1. Introduction

By the start of 20th century, transitions metals (Group IV, V and VI) have attracted many scientists throughout the world as they have exclusive and eccentric properties including their immense hardness, very high melting point, high thermal stability and chemical stability and high corrosion resistance. In the past few decades, nanotechnology has developed rapidly, due to which more and more transition metal carbides are being investigated [1-3]. When these transition metals combine with carbon, they form transition metal carbides (TMCs) or simply carbides. With respect to their parent metals, TMCs behave like noble metals and are utilized for electrochemical reactions such as oxidation of hydrogen, alcohols, and reduction of oxygen. They are generally prepared from metals or metal oxides at high temperatures (~1500 °C or higher) by combining the metal with carbon [1].

1.1 Transition metal carbides (TMCs)

TMCs are also called refractory carbides wherein the general meaning of 'refractory' is the substance which can withstand high heat. Refractory carbides are very useful materials with various industrial applications as they can withstand a high temperature (>1800 ºC) with an ease. Due to high melting points, they can be used under very wide operational temperature ranges and exhibit an unusual mixture of metallic, ionic and covalent behavior. Although, many of the applications of the carbides are recently discovered but the refractory carbides and nitrides have been acknowledged by the scientists for more than a hundred years. As early as the start of 19th century, carbides were being produced such as titanium carbide (TiC) and tungsten carbide (WC) were extracted from steel [1]. In 1890, E. G. Acheson fabricated silicon carbide (SiC) and gave the name Carborundum. By the year 1900, Henri Moissan a French chemist synthesized many carbides by the process of electric arc-furnace [2]. TMCs have many unique properties due to which they find many applications in different industries such as, tantalum carbide (TaC) has very strong covalent bonds and high degree of stability, thus it can be used to enhance performance of very hard metal machining tools [3]. Chromium carbide (Cr_3C_2) is used to manufacture steels, valve seats and is also used as a corrosion resistant material [4]. Silicon carbide (SiC) and boron carbide (B_4C) are used as abrasives in finishing and grinding processes. TMCs are also thermally efficient materials and for that purpose, they are being used in resistors and semi-

conductor devices [5]. Titanium-carbo nitride powder (TiNC), is used in hardening of materials and also for the protection of cutting and sliding surfaces. Alongside, it is also used as a non-toxic cover for medical implants [6]. Zirconium carbide (ZrC) is used in cutting tools (due to its high hardness) and is also used as an applicant for coating of nuclear fuels [7]. Carbides are generally classified in 4 categories on the basis of their bonding between metal and C atoms, these categories are explained in Fig. 1.1 [1].

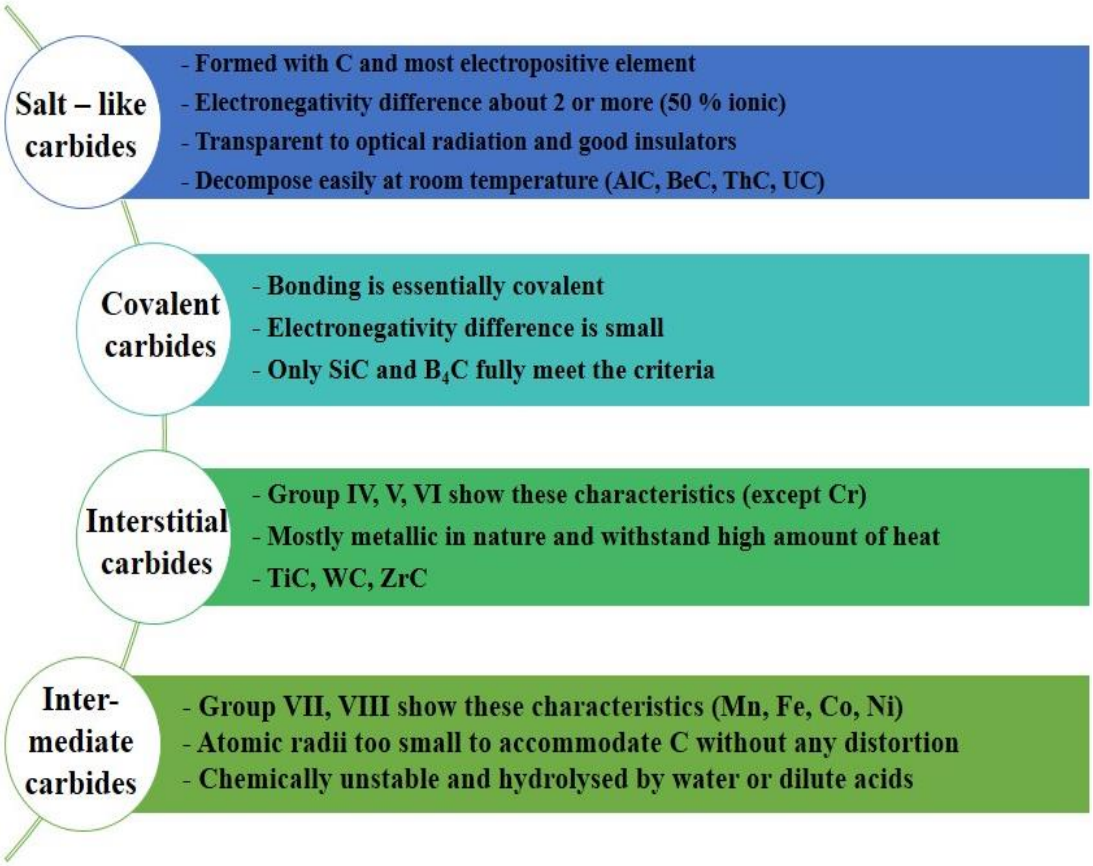

Figure 1.1: Categorization of carbides based on bond nature.

1.2 Applications of TMC's

Carbides find use in various kind of industries, some of them are listed below:

Tungsten carbide (WC) – It has HCP structure and is considered among the hardest carbides with 2600 VHN and 650 GPa bulk modulus. Due to its high hardness it is being used for making machining tools.

Silicon carbide (SiC) – It also has HCP structure and possesses mainly two phases; α (SiC) is the one having non – cubic (hexagonal and rhombohedral) structure and β (SiC) is the

one having cubic structure. It is found in nature as an extremely rare mineral 'moissanite'. The synthesis of SiC is reported back to 1890 by Edward Acheson [8]. It has very high melting point (~2830 ºC). It is widely used as abrasive in lapidary and in the process of whiskering and also in ballistic vests.

Boron carbide (B_4C) – Till 1930, the chemical composition estimated for boron carbide corresponds to formula B_4C but since it has B_{12} structural unit, the chemical formula written for the 'ideal' boron carbide was $B_{12}C_3$. It absorbs neutrons without forming long-lived radionuclides. Also, it is used as an absorbent for neutron radiation which arises in the nuclear power plants and also from anti-personnel neutron bombs. As of 2015, B_4C is the third hardest substance known to the mankind, after diamond and cubic boron nitride, and its nicknamed "black diamond".

Hafnium carbide (HfC) – It is a carbide with melting point of ~3900 °C and is considered as one of the most refractory binary compounds. It also has a low oxidation resistance (starting from 430 °C). Its usages are limited due to high costs, while it is mainly used in hard coatings applied by processes like plasma spraying.

Zirconium carbide (ZrC) – It is a cubic structured carbide with a very high melting point (~3500 ºC) and very high hardness. It has a low neutron absorption cross-section. When placed under radiation it has a very weak damage sensitivity and for this it is used for the coating of thorium dioxide and uranium dioxide particles. Also, due to its high hardness it is being used in cutting tools.

1.3 Crystal Structure and composition

A crystal is defined as a solid material in which the unit cells are arranged in a 3-D manner. In TMCs, the atoms are packed in such a way that they occupy a minimum space. This observable fact is known as close packing. In these kind of structures, the closely packed atoms gets themselves adjusted in the depressions of the other adjacent planes. Therefore, each atom is surrounded by close neighbors, represented as either HCP, BCC, FCC etc. The crystal structures become increasingly complex moving from Group IV to VIII. The crystal structure of TMCs is shown in the table 1.1 which reveals that the carbides show FCC structure while their metals are HCP and BCC. This transition in the crystal can be explained on the basis of number of valence electrons in carbon which further increases the concentration of sp electrons. Group IV compounds follows this trend due to MX

stoichiometry, group V compounds contain high non-metal content and high sp electron density, so in those cases FCC is observed. In early transition metals MX and M_2X are dominant while in later transition metals stoichiometry shifts to M_3X and M_4X.

Table 1.1: Crystal structure of transition metal (M) and their carbides (MC).

Metal	M structure	MC structure
Titanium	HCP	FCC
Zirconium	**HCP**	**FCC**
Hafnium	HCP	FCC
Vanadium	BCC	FCC
Niobium	BCC	FCC
Tantalum	BCC	FCC
Chromium	BCC	ortho-rhombic
Molybdenum	BCC	ortho(α), HCP (β)
Tungsten	BCC	HCP

Most of the TMCs of group IV and V have FCC unit cell in which regular lattice sites are occupied by metal atoms and octahedral voids are occupied by carbon atoms which is shown in schematic diagram (figure 1.2).

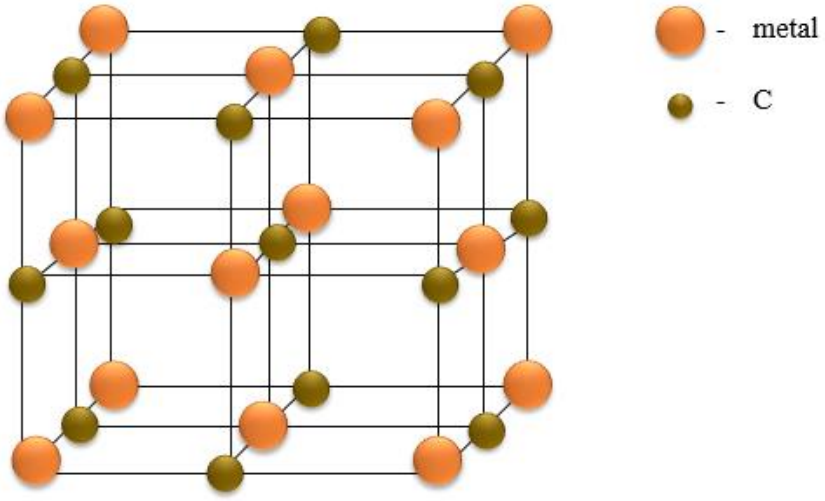

Figure 1.2: Crystal structure of FCC TMCs.

Some of the basic features of TMCs of group IV, V are discussed as follows:

Group IV: This group has the lowest carbon to metal (C/M) atomic radii ratio as compared to group V and VI. The C/M ratio decreases as the size of metal atom increases. They are composed of metal-carbon combination where the C atoms are placed at octahedral sites.

Group V: This group has the intermediate C/M atomic radii ratio as compared to group IV and VI and the C/M ratio decreases as the size of metal atom increases. They are composed of metal-carbon combination where the C atoms are placed at half of the octahedral sites. The main composition is M_2C.

Group VI: This group has the highest C/M atomic radii ratio compared to group IV and V and the C/M ratio decreases as the size of metal atom increases with the exception of Cr as it belongs to the intermediate class of carbides but it meets the refractory criteria. They have many compositions (e.g. Cr have compositions $Cr_{23}C_6$, Cr_7C_3, Cr_3C_2).

1.4 Physical properties of TMCs

1.4.1 Melting point

TMCs are known for their high melting points. Many of the carbides either melts or gets decomposed when reaching above 3000 ºC, TaC having the highest value of ~3900 °C. Group VI elements have the highest range of melting points, but in the case of carbides, the maximum range of high melting points can be found in group V. It is worth noticing in

figure 1.3 that there is an increase in the melting temperature of metals from Ti to W. However, their corresponding carbides show decrease in the melting point.

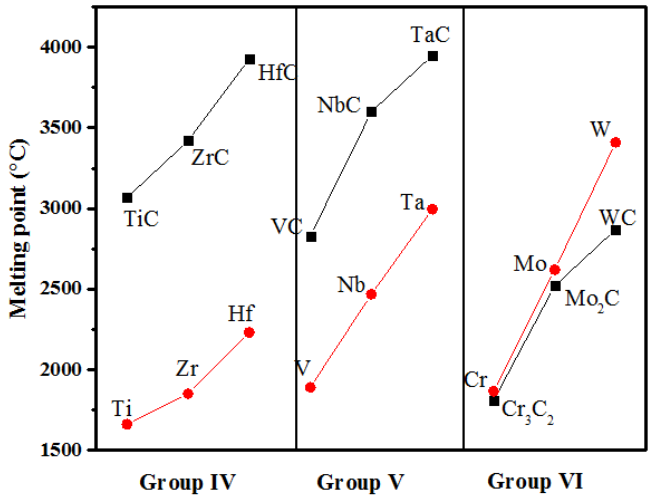

Figure 1.3: Comparison of melting points of TMs and TMCs.

1.4.2 Density

Transition metals of group V and VI have BCC crystal structure while on the other hand Ti and Zr have HCP structure. Most of these transform into FCC structure on carburization. The negative deviation in density of carbides is the cause for this. TiC and ZrC both have higher density than their respective metals. The result of this is an increase in metal – metal spacing which occurs when a mono carbide is formed. The density of metal carbides of group IV, V and VI with their corresponding carbides is shown in Figure 1.4.

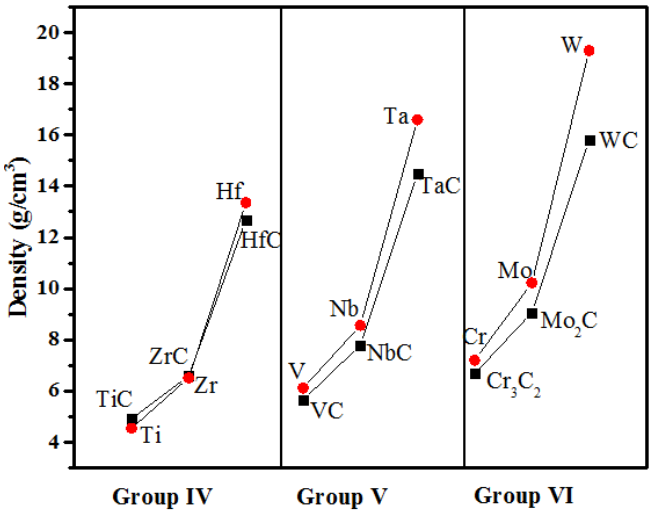

Figure 1.4: Comparison of densities of TMs and TMCs.

1.5 Resistivity

All the materials are basically classified into conductors, semiconductors and insulators. Conductors have the lowest resistivity 10^{-2} - 10^{3} μΩ-cm, while semiconductors resistivity ranges from 10^{6} - 10^{11} μΩ-cm, and insulators have resistivity of about 10^{13} - 10^{18} μΩ-cm. Though, the resistivity of carbides have high value than that of metals, still their resistivity lies in the range of conductors. WC and TaC have the minimum value of resistivity of the range ~22 μΩ-cm while, Cr_3C_2 and TiC have the maximum value of resistivity of the range ~68 μΩ-cm. All the other metal carbides have resistivity in the range of 35-60 μΩ-cm [9].

1.6 Mechanical properties

Mechanical properties mainly include hardness, toughness and stiffness. As hardness involves elastic and plastic deformations, the carbides of group IV have better resistance than groups V and VI. Stiffness may be defined as force applied per unit deformation of the object; the extent to which it resists deformation in response to an applied force. Li ***et al.*** studied that with rise in temperature, the open porosity of the C/ZrC composites increased. As a result of this a strong interface was formed and C fibers got damaged, showing adverse mechanical properties. As a result of this, the strength and toughness decreased from 232 MPa to 103 MPa and from 11.9 MPa $m^{1/2}$ to 3.4 MPa $m^{1/2}$ respectively. There was an increase in the linear recession from 21.0 mm/s to 32.0 mm/s and then to 35.7 mm/s [10].

1.7 Chemical properties

TMCs like platinum (Pt), palladium (Pd) are used as electrode elements in fuel cells and in electrolyzers. WC has been studied extensively as electrocatalyst for oxygen reduction reaction (ORR), methanol oxidation reaction (MOR) and hydrogen oxidation reaction (HOR), and hydrogen evolution reaction (HER) [11-13]. Table 1.2 shows the various characteristic properties of TMCs of group IV, V and VI.

Table 1.2: Comparison data of the TMCs of group IV, V and VI [1].

Property / Carbide	Crystal Structure	Melting Point (°C)	Density (gm/cm^3)	Cond. (W/m-K)	Resistivity (μΩ-cm)	Vicker's Hardness (GPa)	Young's modulus (GPa)	Heat of formation (KJ/mole)	Thermal exp. coeff. ($\times 10^{-6}$/°C)
TiC	FCC	3067	4.91	21.0	50	31.5	410-510	184.6	7.4
ZrC	**FCC**	**3400**	**6.59**	**20.5**	**45**	**25.5**	**350-440**	**196.0**	**6.7**
HfC	FCC	3928	12.67	20.0	41	26.1	350-510	209.6	6.6
VC	FCC	2830	5.65	38.9	60	27.2	430-450	102.6	7.2
NbC	cubic	3600	7.85	14.2	35	19.6	338-580	140.6	6.6
TaC	cubic	3950	14.5	22.1	25	16.7	285-560	142.7	6.3
Cr_3C_2	ortho-rhombic	1810	6.74	19.0	75	14.0	155-245	23.0	10.4
Mo_2C	ortho(α), HCP (β)	2520	9.06	21.5	71	18.5	535-550	23.0	7.9
WC	HCP	2870	15.8	63.0	22	22.0	620-720	40.5	7.3

1.8 Zirconium – carbon (Zr-C) system

As early as 1865, ZrC was prepared from zirconia (ZrO_2) and carbon by Troost [15]. Two decades later, Moissan in 1893 prepared carbides by the reaction in the electric arc furnace [16]. Early ZrC was only prepared by reduction of zirconia which included 3 steps with the formation of Zr_2O_3 which begins to form at 940 – 960 ºC, then ZrO which forms above 1240 ºC, and finally the carbide. The overall reaction is best written as:

$$\mathbf{ZrO_2 + 2.63C \longrightarrow ZrC_{0.71}O_{0.08} + 1.92CO} \quad \textbf{(i)}$$

Zirconium carbide (ZrC) falls under the category of interstitial TMCs with hardness value of the range ~26 GPa due to which it is used in cutting tools and for the coating of wear-resistant materials. It has good thermochemical and thermomechanical properties [17, 18]. Besides having high value of melting point and high hardness ZrC also demonstrates high emissivity. The current carrying capacity of this compound is also very high at higher temperatures. Therefore, ZrC is used in tips of field emitters, photovoltaic radiators and arrays [17-21]. ZrC as the recent studies shows, can be synthesized at low temperature by using the precursors which are prepared by solution-based methods [22-26] which have many advantages. In these kind of methods precursors that are rich in C and Zr are mixed to produce very minute powders, fibers and thin films. Table 1.3 shows the reaction of ZrC with other metals which were taken at different temperatures.

Table 1.3: Reaction of ZrC with metals and metal oxides [14-16].

Metal	Temperature (°C)	Product
Niobium	1600	Forms ZrC – NbC solid solution
Tantalum	2200	Forms TaC and solution of Zr in Ta. It had hardness greater than Ta
Molybdenum	1900	Forms a new phase similar in hardness to Zr
Tungsten	2200	Forms a new phase of great hardness exceeding that of tungsten
Rhenium	2000	Very slight solubility of Re in ZrC (<0.8 at. %) is observed
ZrO_2	1800	Forms an oxycarbide of the type ZrC_xO_{1-x}

1.9 Phase relationship of Zr-C system

ZrC system is a face centered cubic compound. A phase diagram based on a number of studies is shown in figure 1.5.

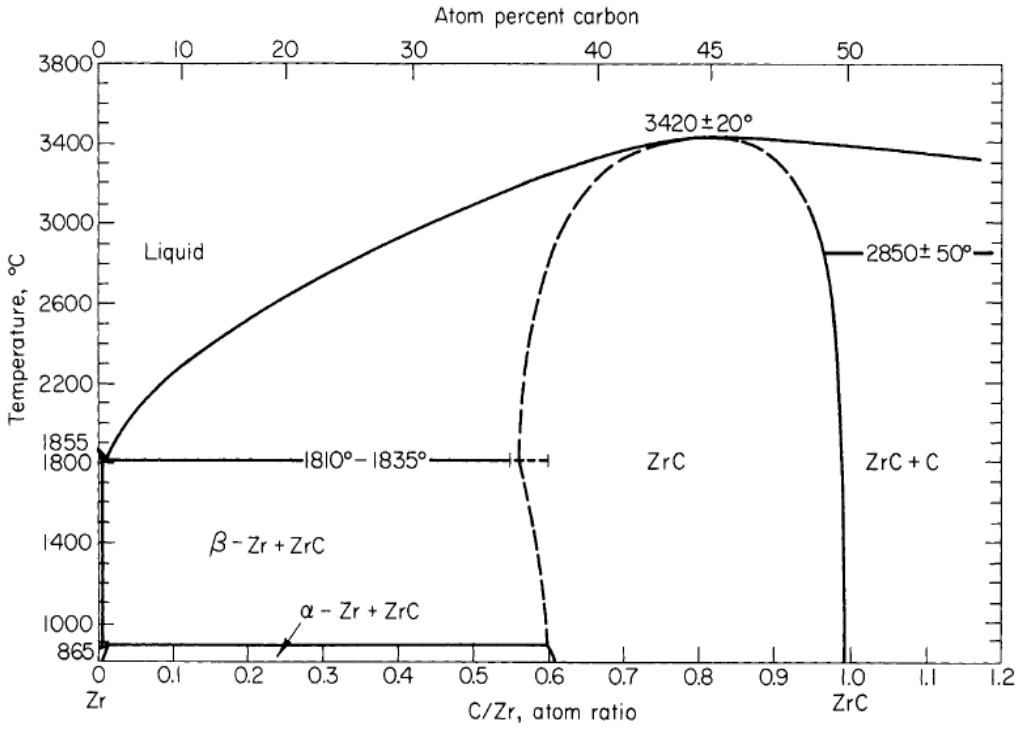

Figure 1.5: Phase diagram of Zr-C system [27].

The melting point of Zr metal is 1855 ± 15 ºC as shown in the figure. Like most of the carbides ZrC is also sub-stiochiometric and contains carbon vacancies and and is stable for C/M ratio 0.65 to 0.98 as is clear from phase diagram and the melting point reaches its peak of 3420 ºC near C/M = 0.8 and then decreases as we move towards higher C/M ratio.

1.9Properties of zirconium carbide

1.9.1 Lattice parameter and density

C. Kempter and R. Fries calculated the lattice parameter for ZrC and found it to be precise to 4.69764 ± 0.00005 Å [28]. They also found that Zr contained 0.5-2% Hf as an impurity, however, they showed such a small amount of Hf has little effect on the lattice constants of zirconium or its compounds. The lattice parameter mainly depends on the rate and amount of the carbon diffusion into ZrC lattice. ZrC has a less value of density (6.73 g/cm^3) compared to other carbides like WC, TaC and HfC [29]. ZrC is used in re-entry

vehicles, rocket/SCRAM jet engines and supersonic vehicles. It fulfils the requirement of the industry which needs less dense materials which can bear high loads at high temperatures.

1.9.2 Chemical reactivity

The chemical reactivity of ZrC is somewhat greater than that of similar carbides e.g. TiC. It is essentially inert to cold concentrated HCl, H_2SO_4, H_3PO_4, $H_2C_2O_4$, $HClO_4$, and H_2SO_4 + H_3PO_4. However, cold HNO_3, HCl + HNO_3, or dilute H_2SO_4 + H_3PO_4 and the oxidizing acids when heated, dissolves the carbide. The reaction between CO and ZrC leads to an oxycarbide. Prescott (1926) measured the pressure of CO over a mixture of ZrO_2, C, and ZrC [30]. This data was represented by the equation taken in the temperature (T) range 1600-1750 ºC:

$$\log P\,(CO) = 8.592 - (16580/T) \qquad \textbf{(ii)}$$

1.9.3 Heat of formation

Mah and Boyle (1955) reported the value of heat of combustion as -44.1 ± 1.5 kcal/mole for an impure sample of ZrC for which two assumptions were made for correcting ZrC results. First, the sample was assumed to be 94.01% ZrC, 5.86 % ZrN and 0.13% free C which lead to 72.7 cal /g correction. Secondly, it was assumed that the sample contained 94.72% ZrC, 5.23% ZrO and 0.05% free C which lead to 92.0 cal /g correction [31]. A decade later Mah (1964) found the value to be -47.0 ± 0.6 kcal/mole for two samples; one analyzing $ZrC_{0.93}$ (with 0.11% free C, 0.18% N and 0.17% O_2) and the other $ZrC_{0.99}$ (0.12 % Ti, 0.07 %N and 0.05% O_2). Mah assumed that the oxygen was present as ZrO_2, and Ti and B were uncombined. If, on the other hand, the oxygen were dissolved as $ZrO_{0.7}$ and boron as $ZrB_{0.7}$, and the titanium as $TiC_{0.7}$, heat of formation of -30.8 kcal/mole for $ZrC_{0.73}$ was obtained.

1.10 Advantages of zirconium carbide over other TMCs

ZrC is a very important compound as it has a high corrosion resistant capacity. ZrC is also a member of ultra-high temperature ceramics or the UHTC community. Due to covalent bonding ZrC has a very high melting point than the other carbides. The main advantage of this compound is its low value of density (~6.8 g/cm^3) which makes it suitable for the use in re-entry vehicles, rocket/SCRAM jet engines and supersonic vehicles. As mentioned

earlier when compared to other carbides, it has a low neutron absorption cross-section due to which it is used as the coating of thorium and uranium dioxide particles. The application of ZrC in hard alloy can improve the hardness and corrosion resistance of materials. ZrC nanoparticles can be used in nano-structured parts in metallurgical, chemical and aviation industries. It finds its application in the textile industry in making thermostat textiles in nylon, fiber and hard alloy. Besides all this, ZrC nano powders has high visible light absorption, excellent infrared reflectance and large energy storage characteristics [32]. Due to some superior characteristics over other TMCs, it can revolutionize various engineering sectors if ZrC can be synthesized optimally at low temperatures.

1.11 References

1. Pierson H. O., Handbook of refractory carbides and nitrides, Noyes Publications, U.S.A, 1996.
2. Moissan H., Le carbure de calcium et l'acétylène, Comptes Rendus Acad. Sci, 1 (1897) 322-322.
3. Palomar F.E., Zambrano P., Gómez M. I., Colás R., Castillo A., Tungsten carbide and tantalum carbide coatings on machining tools, Ingeneria Mecanica Tecnologia Y Desarrollo, 84 (10) (2010) 1236-1239.
4. Natesan K., Johnson R., Corrosion resistance of chromium carbide coatings in oxygen-sulfur environments, Surface and Coatings Technology, 33 (1987) 341-351.
5. Matus L., Powell J., Petit J., Development of silicon carbide semiconductor devices for high temperature applications, NASA Technical Memorandum, 104398 (1991).
6. Ching H., Choudhury D., Nine Md., Osman N., Effects of surface coating on reducing friction and wear of orthopaedic implants, Sci. Technol. Adv. Mater. 15 (1) (2014) 1-22.
7. Katoh Y., Vasudevamurthy G., Nozawa T., Snead L., Properties of zirconium carbide for nuclear fuel applications, J. Nuc. Mat. 441 (1-3) (2013) 718-742.
8. Acheson, E.G., To the Carborundum Co. U.S. Patent 492, (Feb. 28 1893), 767.
9. Oyama S. T., The chemistry of transition metal carbides and nitrides, Blackie Academic and Professional, Glasgow (1996).
10. Li Y., Chen S., Ma X., Hu H., Zhnag Y., Influence of preparation temperature on the properties of C/ZrC composites, J. All. & Comp. 690 (2017) 206-211.
11. Chen W., Muckerman J., Fujita E., Recent developments in transition metal carbides and nitrides as hydrogen evolution electrocatalysts, Chem. Commun. 49 (2013) 8896-8909.
12. Vasic D., Pasti I., and Mentus S., DFT study of platinum and palladium overlayers on tungsten carbide: structure and electrocatalytic activity toward hydrogen oxidation/evolution reaction, Int. J. Hydrogen Energy, 38 (12) (2013) 5009-5018.

13. Weigert E., Stottlemyer A., Zellner M., Chen J., Tungsten monocarbide as potential replacement of platinum for methanol electro-oxidation, J. Phys. Chem. C, 111(40) (2007) 14617-14620.

14. Samsonov G., Strashinskaya L., Shiller E., Izv. Akad. Nauk USSR, Otd. Tekh. Nauk, Met. Toplivo, 5 (1962) 167-167.

15. Troost L., Pechard E., Traitè elèmèntaire de chimie comprenant les prinicpales applications à l hygièaux arts et á/ hygièaux arts et á l'industri, Paris, 24th rev. ed (1865).

16. Moissan H., Chimie Minérale – Description d'un nouveau four électrique, Comptes rendus hebdomadaires des séances de l'Académie des sciences, 115 (1892) 1031.

17. He X., Shu L., Li H., Weng D., High corrosion resistant ZrC films synthesized by ion-beam-assisted deposition, J. Mater. Res., 14(2) (1999) 615-618.

18. Reynolds G., Janvier J., Kaae L., and Morlevat J., Irradiation behavior of experimental fuel particles containing chemically vapor deposited zirconium carbide coatings, J. Nuc. Mat., 62 (1) (1976) 9-16.

19. Sheats J., Mackie W., Anz S., Xie T., Polymer electroluminescent devices with zirconium carbide cathodes, Society of photographic instrumentation engineers (SPIE) 3148 (1997) 219-227.

20. Charbonnier F., Mackie W., Hartman R., Xie T., Robust high current field emitter tips and arrays for vacuum microelectronics devices, J. Vac. Sci. Technol. B, 19 (3) (2001) 1064-1072.

21. Cockeram B., Measures D., and Mueller A., The development and testing of emissivity enhancement coatings for thermophotovoltaic (TPV) radiator applications, Thin Solids Films, 17 (1999) 355-356.

22. Sarkar S., Miller A., Mueller J., Solubility of oxygen in ZrC, J. Am. Ceram. Soc., 55(12) (1972) 628-630.

23. Kurokawa Y., Ota H., Sato T., Preparation of carbide fibers by thermal decomposition of cellulose-metal (Ti, Zr) alkoxide gel fibers, J. Mater. Sci. Letters, 13 (7) (1994) 516-518.

24. Kurokawa Y., Kobayashi S., Suzuki M., Shimazaki M., Takahashi M., Preparation of refractory carbide fibers by thermal decomposition of transition metal (Ti, Zr, Hf, Nb, Ta) alkoxidecellulose precursor gel fibers, Mater. Res., 13(3) (1998) 760-765.

25. Hasegawa I., Fukuda Y., Kajiwara M., Inorganic-organic hybrid route to synthesis of ZrC and Si-Zr-C fibers, Ceram. Int. 25 (6) (1999) 523-527.

26. Preiss H., Schierhorn E., Brzezinka K., Synthesis of polymeric titanium and zirconium precursors and preparation of carbide fibers and films, J. Mater. Sci., 33 (19) (1998) 4697-4706.

27. Storms E.K., The refractory carbides, Academi Press Inc. ltd., London (1967).

28. Kempter C., Fries R., Crystallographic Data. 189. zirconium carbide. Analytical Chemistry, 32 (4) (1960) 570-570.

29. Lide D., CRC Handbook of Chemistry and Physics (90th ed.) Boca Raton, Florida (2009).

30. Prescott C., The equilibrium between zirconium oxide and carbon and their reaction products at incandescent temperatures, J. Am. Chem. Soc., 48 (10) (1926) 2534–2550.

31. Mah A., Boyle B., Heats of formation of niobium carbide and zirconium carbide from combustion calorimetry, J. Am. Chem. Soc., 77 (24) (1955) 6512–6513.

32. Blog on The application of ZrC powders, Stanford advance materials, http://www.samaterials.com/content/137-the-application-of-zirconium-carbide-powder (2016).

2. Literature Review

Among all the known TMCs, zirconium carbide (ZrC) holds special importance as it is used for cutting tools and other industrial purposes. Synthesis of ZrC is also a perilous process as its properties is dependent mainly on the procedure followed for the synthesis. ZrC was prepared as early as in the 1960's [1]. Some of the important developments on the formation of ZrC is being discussed as follows.

In 1972, **Sarkar *et al.*** [2] took a mixture of reactor-grade ZrO_2 and graphite. Heat treatment was given to the sample in a specially designed graphite tube furnace. The reactions between ZrO_2 and C were carried from 1400 to 1800 °C in the presence of CO. The pressures ranged from 100-760 Torr with holding time from 4 to 75 h. The as-synthesized samples had zirconium oxycarbide (ZrC_xO_y) as an intermediate phase in which ZrO_2 and C didn't react. The lattice parameter 'a' of the intermediate phase observed was in between 0.4676 to 0.4681 nm depending on various heat treatment cycles followed.

In 1990, **Lu *et al.*** [3] prepared ZrC by using $(RO)_4Zr$ as a liquid organometallic precursor. The reaction was performed in a newly developed mechanism called Triple Torch Plasma Reactor (TTPR) in temperature range of 1500 to 3500 °C. It was suggested that excess C can be removed with the addition of a fixed amount of CO_2 in the plasma. The product powder was porous and spherical with the specific area of 140 m^2/g.

In 1993, **Kobayashi *et al.*** [4] investigated the conditions for low-temperature synthesis of ZrC fine powder from ZrO_2-Mg-CH_4 reaction which was cyclic in nature. The synthesis was performed with the help of thermite-type reaction which is conducted in pure Ar atmosphere, with metallic Mg as reducing agent and CH_4 gas as a carbon source. Single phase ZrC was formed through the formation and decomposition of Mg_2C_3 ($2Mg + 3CH_4 + Mg_2C_3 + 6H_2 \rightarrow 2Mg + 3C$) with a molar ratio of 2.2:1 ($Mg:ZrO_2$) at 750 °C for 30 min. The average particle size was 0.05 µm with specific surface area measured via BET was in the range of 44.1 - 49 m^2/g.

In 1997, **Tsuchida *et al.*** [5] used planetary ball mill to synthesize ZrC nanopowders using various molar ratios of Zr and C. The mixed Zr and C powders was exposed to air in graphite crucible via self-propagating high-temperature synthesis (SHS). Morphology, color and phase composition of final products were observed for Zr-C powder mixtures with varying amounts of carbon content. The structures obtained were stratified swelling type structure, porous swelling type structure and

block-like structure without swelling depending upon the carbon content. The carbon content also affected the crystal structure of ZrC with variable lattice constant from 0.4637 - 0.4693 nm.

In the same year, **Maitre and Lefort** [6] performed a solid–solid reaction between zirconia and carbon under inert Ar atmosphere thereby producing ZrC by the formation of intermediate oxycarbide $ZrC_{0.84}O_{0.06}$. The mixtures obtained were kept in carbon crucibles followed by heat treatment of the samples in the presence of Ar at temperatures ranges of 1350 to 1550 °C. The completion of the reaction took place at 1450 °C when the sample was kept for 12h. Thermal analysis were performed to check the rate of the reaction and lattice parameter was also calculated. Temperature was optimized within the range of 1350 to 1550 °C, and it was observed that the final transformation of the oxycarbide into carbide was slow. Lattice parameter remained constant even with variation in the temperature having the value of 0.4688 nm.

In 1999, **Hasegawa *et al.*** [7] mixed phenolic resin and zirconium 2, 4,-pentanedionate (ZTP) in 2,4 pentanedione and ethanol, 10ml each, with the addition of sulphuric acid and distilled water. C/Zr molar ratio was kept at 4.0 in the initial stages. The solutions were stirred at room temperature at 65 °C for half hour. The dried fibers were heat treated at different temperatures in between 1100 to 1500 °C for 4h in Ar atmosphere. However, samples prepared at 1500 °C showed single phase ZrC in the XRD spectrum.

In 2002, **Dong *et al.*** [8] synthesized ZrC by mixing zirconia and graphite in a ball mill for 24 h. The as-synthesized powders were heat treated at 1800 °C in vacuum furnace at 100 Pa N_2 pressure. Due to longer duration and high energy of the milling process ZrO_2 powders were able to react with carbon at room temperature.

In the same year, **Li *et al.*** [9] synthesized nano ZrC via a reduction-carburization process in which they took 6.9 g $ZrCl_4$, 3mL CCl_4 and 5.1g granular Na metal into an autoclave made of stainless steel. The autoclave was sealed and heated to 550 °C for 12h. The sealed autoclave was then cooled down to room temperature. The as-synthesized sample was washed with ethanol, 0.1M HCl and distilled water. This was done to remove NaCl and other impurities. The sample was then dried in vacuum oven at 60 °C for 4h. XRD of the sample confirmed face-center cubic (FCC) ZrC having a = 4.686 Å, while the average size of nanocrystallites were 18 nm, which was estimated from the Debye-Scherrer formula. The SAED pattern suggested that particles were well-defined single crystal while, HRTEM micrographs showed regular fringe spacing with 0.238 nm corresponding to (002) plane having a graphite coating. Thermodynamic calculations revealed

that reduction reactions of $ZrCl_4$ and CCl_4 with Na were spontaneous and exothermic. This was confirmed by the negative values of ΔG and ΔH with the starting temperature of 400 °C.

In 2004, **Shen *et al.*** [10] synthesized ZrC nanospheres by taking $ZrCl_4$, C_6Cl_6, and Na as precursors in an autoclave at 600 °C for 20 h. The samples were washed several times with C_2H_5OH and then with distilled water for the removal of impurities including NaCl. XRD confirmed the formation of ZrC with a measured lattice parameter of a = 0.4861 nm and TEM micrographs confirmed the diameter of the nanoparticles in the range of 50-80 nm.

In 2007, **Yan *et al.*** [11] prepared ultrafine ZrC via a new route called the sol-gel method using zirconium oxychloride ($ZrOCl_2{\cdot}8H_2O$) as Zr source and phenolic resin as the carbon source. 0.2 moles per litre of $ZrOCl_2{\cdot}8H_2O$ was prepared by dissolving some $ZrOCl_2{\cdot}8H_2O$ in the solution such that C_2H_5OH/H_2O ratio was about 4:1. Some adjustments were done in the pH value using dilute NH_3 by stirring it continuously to form a zirconia sol. After which phenolic resin was added in the molar ratio of 3:1 of C/ZrO_2 to form a binary sol. The obtained gel was put in a jar and ball milled for 24h and then kept in open for 4h. A binary gel was formed which was dried in the oven for 12h at 80 °C. The reactions were done at 1400 °C/1h. The average crystallite size of the particles was less than 200 nm with a specific area of 54 m^2/g. The measured oxygen content of the synthesized powder at 1400 °C/1h was less than 1.0 wt%.

In the same year 2007, **Dolle *et al.*** [12] also synthesized ZrC via sol–gel route. Zirconium *n*-propoxide, saccharose as carbon source and acetic acid were mixed forming a gel. These gels were subjected to pyrolysis under Ar atmosphere thereby obtaining the desired precursors which contained mixed nanosized tetragonal ZrO_2 and amorphous C. When these mixtures were further heat treated, the precursors had carbothermal reduction of the oxide particles and then oxycarbides were formed. It was proved that the oxygen content of the particles can be decreased by increasing the temperature from 1400 °C (8 at. %) to 1600 °C (3 at. %).

In 2010, **Lee *et al.*** [13] developed a novel reduction method to obtain ZrC powders. $ZrCl_4$ was used as Zr source while carbon black as carbon source. Sodium bicarbonate ($NaHCO_3$) was used as a reducing agent [13]. To reduce the amount of Cl in $ZrCl_4$ by Na component in $NaHCO_3$ ball-milling process was used, which further lead to the formation of sodium chloride. Synthesis parameter (temperature) was varied. Also, the various molar ratios of initial carbon content were optimized. It was found out that when 1 mole of $ZrCl_4$ and 6 moles of $NaHCO_3$ were used as the

starting precursors, the Zr/C ratio initially required to produce pure ZrC was about 7 moles. ZrC phase was synthesized at 1400 °C with 150 nm as average crystallite size.

In 2010, **Tao *et al.*** [14] took preceramic polymer, polyzirconoxanesal (PZS) and synthesized it efficiently by one-pot protocol (strategy to improve efficiency of a chemical reaction). Various characterizations like gel permeation chromatography (GPC), nuclear magnetic resonance (^{1}H-NMR and ^{13}C-NMR) and Fourier transform infrared spectra (FTIR) were performed. The formation of the precursor revealed excellent solubility for processing fiber composites. Pyrolytic conversion was studied with the help of thermogravimetric analysis (TGA), along with XRD and scanning electron microscopy (SEM). Decomposition of the polymer was completed at 600 °C and at 1300 °C, ZrC was achieved. The experiment was performed in the presence of Ar with the total yield of the final sample being 68.5%. According to the authors, 1300 °C was the lowest temperature for preparing ZrC ceramics by using these kind of precursors. The spherical shaped ZrC particles had sizes in the range of 20 to 100 nm. The phase transition from t-ZrO_2 to m-ZrO_2 occurred from 600 to 1200 °C while, pure ZrC was formed at or above 1300 °C.

In 2011, **Xiang *et al.*** [15] synthesized activated zirconium carbide nanoparticles at room temperature via mechano-chemical route by making use of ball milling technique. During the milling, toluene served as a Process Control Agent (PCA) as well as a source of carbon. The carbon content (*x)* can be changed accordingly by controlling the time of ball milling. The ZrC_x nanoparticles at 1200 °C showed a Vicker's hardness of ~14 GPa. These spark plasma sintered particles had density of ~99.8%. Other carbides like WC_x, TiC_x, and NbC_x, can also be prepared with the help of this technique.

In 2011, **Chen *et al.*** [16] synthesized ZrC nanoparticles which had average size of about 10 nm using pulsed plasma in liquid (PPL) technique. Zr metal electrodes were the source of Zr and liquid ethanol was used as C source. The effect of quenching and vacuum environment in this method were studied. As a result, highly pure and uniformly distributed samples were obtained. The results of thermo gravimetric analysis (TGA) and infrared ray emissivity showed that the graphite containing carbon shells were composed of several layers. The transmissivity of these layers were very high which protect the ZrC nanoparticle from oxidation and it also preserves its high infrared ray emissivity.

In 2013, **Arianpour *et al.*** [17] synthesized ZrC using zirconium acetate as Zr source, sucrose as carbon source and polyvinyl alcohol as reducing agent. All these were mixed in the presence of

HNO_3 at 80 °C for 2h. Then, the precursor was dried at 200 °C in an oven for 4h. The precursor was then placed in an electric furnace. The heating rate was kept at 10 °C/min with 3h of soaking time with a high vacuum of 10^{-5} Torr. After this, the final products were ball milled after which XRD and SEM were done. Carbon to zirconium ratio (C/Z = 4) contained the highest amount of carbide phase with 20nm crystallite size.

In the same year, **Wang *et al.*** [18] followed auto clave method for the synthesis of ZrC in which ZrO_2 (1.23 g), Li_2CO3 (0.74 g) metallic Mg (2.40 g) were mixed and heated in an autoclave to 600 °C for 20 h. After the autoclave was cooled down to room temperature, the washing of precipitates was done with the help of ethanol, HCl and distilled water for removing the impurities. Drying of the samples was done in a vacuum oven for 5h at 60 °C. XRD showed pure phase ZrC with a lattice constant of 4.693 Å. It was observed that particles were in the range of 20 to 40 nm in diameter. In TGA analysis, it was found that the sample has good thermal stability below 250 °C.

In 2014, **Justin *et al.*** [19] synthesized activated porous ZrC by Na_2CO_3, by the activation of commercial ZrC. As a result, there was a tremendous increase in the specific surface area (from 0.6 to 96 m^2/g) of ZrC which was further incorporated into vulcan carbon XC-72R by solid-state reaction by a method of intermittent microwave heating or IMH, where the heating was performed at irregular intervals and Pt nanoparticles were dispersed. The performance for oxygen reduction reaction (ORR) was studied in 0.1 mol/L $HClO_4$ aqueous electrolyte by cyclic voltametry. XRD, XPS results and TEM micrographs indicated ZrC nanoparticles are dispersed over vulcan carbon XC-72R. On the combination of activated ZrC with Pt, the resulting catalyst showed higher activity for oxygen reduction.

In 2015, **Lei Dai *et al.*** [20] synthesized ZrC via a method of direct electrolysis. They were able to show that the pure ZrC powder can be obtained by direct electrolysis of non-sintered ZrO_2/C mixture in molten $CaCl_2$ (850 °C) at voltage range of 3V for a time period 7h. The C content of the mixture was over stoichiometric ratio of ZrC and C, promoting the electrochemical reduction of ZrO_2 with $CaZrO_3$ as intermediate. A molten salt reactor was used to perform all the electrolysis experiments in the presence of inert (Ar) atmosphere.

Aoyun *et al.* [21] in 2015, fabricated high quality nano-sized ZrC powders via self propagating high-temperature synthesis or SHS method followed by process of ball milling. ZrO_2, Mg as reducing agent and sucrose ($C_{12}H_{22}O_{11}$) as carbon source were charged to ball mill (ZrO_2 balls,

ball to powder weight ratio was 4:1, rotating rate was kept at 400 RPM). The samples were mixed for 3h using alcohol as ball milling medium and then they were dried at 80 ℃ for 12h. The mixture was then pressed into a cylinder which was kept under Ar atmosphere at 800 °C for 10 min. The collected product was washed with dilute HCl, distilled water and ethanol. The samples were then dried in vacuum at 80 °C for 24h. The as-synthesized samples were highly pure, had a very low oxygen content and the particles were evenly distributed. The average particle size of the particles was 50 nm.

In 2016, **Mohammad *et al.*** [22] succeeded in synthesizing ZrC by using $ZrCl_4$ (4.82 g) and naphthalene (2.23 g) by dissolving them in toluene (C_6H_5-CH_3). The reagents were stirred at 100 °C and later on Na (1.95 g) was added into the solution. A brown solid was formed which was then heated in an electric arc furnace under Ar atmosphere for 1h. Impurities were removed by washing the samples in distilled water. The samples were then dried in vacuum at 200 °C for 30 min. The results revealed that after heat treating the samples in Ar atmosphere above 500 °C, $ZrCl_4$ started to form ZrC nanorods which were converted to pure ZrC at 700 °C. The nanorods had cubic lattice structure with the length ranging from 50 to 70 nm. ZrC nanorods are potential candidates for the future and can be used for various purposes such as cutting tools, in high temperature ceramics (HTC) and also in engineering composites including gas turbine blades.

In 2016**, Liu *et al.*** [23] synthesized ZrC by using organic polymer as a precursor. The α-hydroxycarboxylic acid and tartaric acid, formed complex structure with zirconium. This complex reacted with $C_2H_6O_2$ via polyesterification process which immobilized the metal ion [23]. The carbothermal reaction was completely achieved at 1300 ^oC by mixing the precursors with ZrO_2/C (coke). ZrO_2/carbon (coke) gets converted into carbide by forming an intermediate oxycarbide phase. Average particle size was calculated to be in the range (50–150 nm). Thermal analysis of the obtained ZrC powders in air environment showed that the ZrC started to oxidize at 260 ^oC followed by the oxidation of carbon at 680 ^oC.

In 2016, **Sugashima *et al.*** [24] synthesized ZrC by pursed wire discharge (PWD) in Ar, (Ar + oleic acid) fume/vapor and oleic acid liquid. It was a new method for synthesis of ZrC nanopowders by using PWD in organic liquid. XRD pattern showed various planes calculated from the peak positions. The particle size of the as-synthesized samples was calculated with the help of TEM micrographs. It was confirmed that most of the prepared particles were less than

100 nm. By using oleic acid liquid, it was confirmed that particle size was 20.5 nm. Therefore, PWD method in oleic acid was suggested to be effective for the synthesis of carbide nanopowders. In 2017, **Feng *et al.*** [25] synthesized nano-sized ZrC powder at high temperature (1600 °C) by the carbothermal reduction of ZrO_2 using a modified spark plasma sintering (SPS) apparatus. The synthesized ZrC powder had a particle size of approximately 189 nm and a low oxygen content of 0.88 wt%. The metal basis purity of the synthesized powder came out to be 99.87%. Along the experiment, it was noted that low synthesis temperature, faster heating/cooling rates and the effect of current during the modified SPS process suppressed the particle growth effectively. Using the synthesized powder, ZrC ceramics were obtained with high relative density (97.14%) after that they were densified at very high temperature (2100 °C) for 30 min at a pressure of 80 MPa by SPS. The average grain size of the densified ZrC ceramics was approximately 9.12 μm.

2.1 References

1. Moissan H., Chimie Minérale – Description d'un nouveau four électrique. Comptes rendus hebdomadaires des séances de l'Académie des sciences, 115 (1892) 1031-1031.
2. Sarkar S. K., Miller A. D., Mueller J. I., Solubility of oxygen in ZrC, J Am Ceram Soc. 55(12) (1972) 628-630.
3. Lu Z .P., Or T. W., Stachowicz L., Kong P., Pfender P., Synthesis of zirconium carbide in a triple torch plasma reactor using liquid organometallic zirconium precursors, Mat. Res. Soc. Symp. Proc.190 (1990) 77-82.
4. Kobayashi H., Shimosaka K., Saitoh M., Mitamura T., Low-temperature synthesis of ZrC powder by cyclic reaction of Mg in ZrO_2-Mg-CH_4, J. Am. Ceram. Soc.76 (9) (1993) 2389-2392.
5. Tsuchida T., Kawaguchi M., Kodaira K., Synthesis of ZrC and ZrN in air from mechanically activated Zr-C powder mixtures, Solid State Ionics 101-103(1-2) (1997) 149-154.
6. Maitre A., Lefor P., Solid state reaction of zirconia with carbon. Solid State Ionics.104 (1997) 109-122.
7. Hasegawa I., Fukuda Y., Kajiwara M., Inorganic-organic hybrid route to synthesis of ZrC and Si-Zr-C fibres, Ceram. Int.25(6) (1999) 523-527.
8. Dong J, Shen W, Liu X., A new method synthesizing the encapsulated ZrC with graphitic layers, Mater Res Bull. 36(5-6) (2002) 933-938.
9. Li C., Yang X., Zhao Z., Qian Y., A co-reduction-carburization route to synthesize nanocrystalline ZrC. Sci Technol. 2-3 (2002) 1088-1089.
10. Shen G., Chen D., Liu Y., Tang K., Qian Y., Synthesis of ZrC hollow nanospheres at low temperature, J. Cryst. Growth 262 (1-4) (2004) 277-280.
11. Yan Y., Huang Z., Liu X., Jiang D., Carbothermal synthesis of ultra-fine zirconium carbide powders using inorganic precursors via sol-gel method, J. Sol-Gel Sci. Technol. 44(1) (2007) 81-85.
12. Dollé M., Gosset D., Bogicevic C., Karolak F., Simeone D., Baldinozzi G., Synthesis of nanosized zirconium carbide by a sol-gel route, J. Eur. Ceram. Soc. 27(4) (2007) 2061-2067.

13. Lee D., Jin S., Yu J., Lee H., Synthesis of ultrafine ZrC powders by novel reduction process, Mater. Trans. 51(12) (2010) 2266-2268.
14. Tao X., Qiu W., Li H., Zhao T., Synthesis of nanosized zirconium carbide from preceramic polymers by the facile one-pot reaction, Polym. Adv. Technol. 21(4) (2010) 300-304.
15. Xiang J., Liu S., Hu W., Zhang Y., Chen C., Wang P., He J., Yu D., Xu B., Lu Y., Tian Y., Liu Z., Mechanochemically activated synthesis of zirconium carbide nanoparticles at room temperature: A simple route to prepare nanoparticles of transition metal carbides, J. Eur. Ceram. Soc. 31(8) (2011) 1491-1496.
16. Chen L, Iwamoto C., Omurzak E., Synthesis of zirconium carbide (ZrC) nanoparticles covered with graphitic "windows" by pulsed plasma in liquid, RSC Adv. 1(6) (2011) 1083-1088.
17. Arianpour F., Kazemi F., Rezaie H., Asjodi A., Liu J., Nanozirconium carbide powder synthesis via carbothermal route, Defect Diffus. Forum 334-335 (2013) 381-386.
18. Wang L., Si L., Zhu Y., Qian Y., Solid-state reaction synthesis of ZrC from zirconium oxide at low temperature, Int. J. Refract. Met. Hard Mater. 38 (2013) 134-136.
19. Justin P., Charan P., Rao G., Activated zirconium carbide promoted Pt/C electrocatalyst for oxygen reduction, Appl. Catal. B. Environ. 144 (2014) 767-774.
20. Dai L., Wang X., Zhou H., Direct electrochemical synthesis of zirconium carbide from zirconia/C precursors in molten calcium chloride, Ceram. Int. 41(3) (2015) 4182-4188.
21. Da A., Long F., Wang J., Preparation of nano-sized zirconium carbide powders through a novel active dilution self-propagating high temperature synthesis method, J. Wuhan Univ. Technol. Sci. Ed.30(4) (2015) 729-734.
22. Mahdavi M., Ramazani M., Darvishi Z., Synthesis and characterization of zirconium carbide nanorods at low temperature, Int. J. Refract. Met. Hard Mater. 56 (2016) 59-62.
23. Liu R., Yan C., Zhang C., Cao Y., Long X., Synthesis of zirconium carbide nanoparticles by polymerised complex route, Adv. Appl. Ceram.114 (2016) 6753-6761.

24. Sugashima K., Suzuki K., Suzuki T., Nakayama T., Suematsu H., Niihara K., Synthesis of zirconium carbide nanosized powders by pursed wire discharge in oleic acid, J. Korean Phys. Soc.68(2) (2016) 345-350.
25. Feng L., Lee S., Lee H., Nano-sized zirconium carbide powder: Synthesis and densification using a spark plasma sintering apparatus, Int. J. Refract. Met. Hard. Mater. 64 (2017) 98-105.

3. Experimental Work

In the present work, zirconium carbide (ZrC) nanopowders were synthesized following a carbothermal-reduction route using zirconium oxide (ZrO_2, *Sigma-Aldrich, 99.5%*) as Zr source, hexane (C_6H_{14} *95% LR*, SDFC Ltd.) as C source and magnesium (Mg) metal powder (SDFC Ltd.) to reduce ZrO_2 and further to facilitate the formation of ZrC. Detailed description of the materials and methodology is as follows:

3.1 Methodology

All the experiments were performed in a tightened stainless steel autoclave of 30ml capacity in which a mixture of ZrO_2 (1.232 g), C_6H_{14} (10 ml) and Mg (2g) metal powder was mixed in agate-mortar. Heat treatment of the mixture was done at different temperatures (600, 700 and 800 °C). The heating rate was kept at 5°C/min with a holding time of 5h and 10h at each temperature. After heating the autoclave at desired temperature it was cooled at room temperature keeping it in furnace. It was observed that in-situ phase formation occurred at 800 °C. At this temperature variation of carbon content (7ml, 4ml, 1ml, 0.22ml and 0.198 ml) was done to optimize the synthesis parameters. In the later stages, holding time was also varied to 2.5h and 7.5h as an attempt to check for any change in phase composition mechanism. In each of the cases, leaching of the as-synthesized powder was done by taking a solution of HCl : H_2O (1:1) for the removal of undesired MgO and other metastable impurities. Finally, the powder was subjected to wash several times with the help of distilled water, after which it was kept in oven for drying at 120 °C for a time period of 24h. Table 3.1 shows the experimental data consisting of different synthesis conditions:

Table 3.1: Data of the experimental conditions for preparing ZrC nano powders.

Sample Id	(C_6H_{14}) (ml)	Temperature (°C)	Holding time (h)
5ZrC600	10	600	5
10ZrC600	10	600	10
5ZrC700	10	700	5
10ZrC700	10	700	10
2.5ZrC800	10	800	2.5
5ZrC800	10	800	5
7.5ZrC800	10	800	7.5
10ZrC800	10	800	10
5ZrC800 C7	7	800	5
5ZrC800 C4	4	800	5
5ZrC800 C1	1	800	5
5ZrC800 C0.22	0.22	800	5
5ZrC800 C0.198	0.198	800	5

The process followed is shown in figure 3.1 below, which represents the formation of ZrC nano powders, in which, initial, intermediate and final conditions are mentioned.

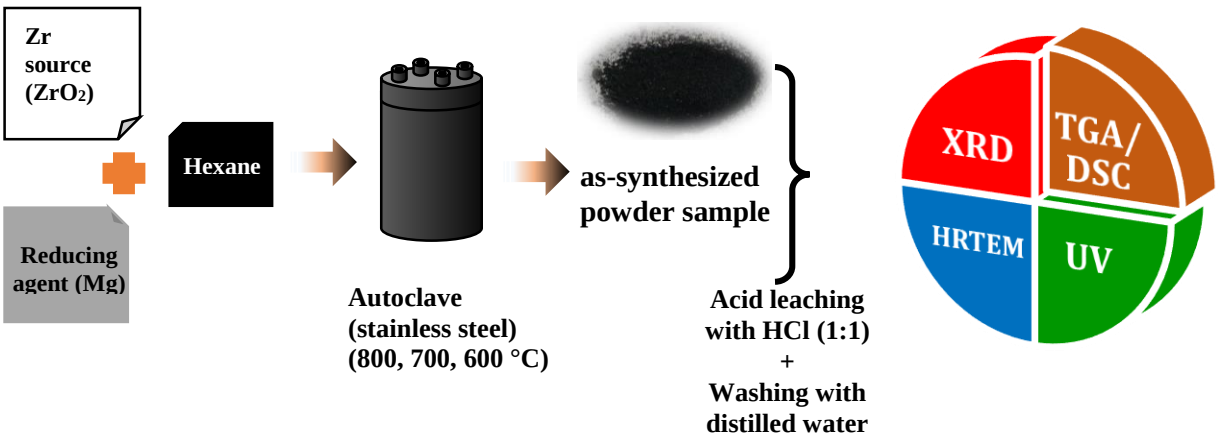

Figure 3.1: Methodology for synthesizing and characterizing nano zirconium carbide (ZrC).

3.2 Characterizations

3.2.1 X-ray diffraction (XRD)

XRD is an indispensable method for characterization of a material, making use of the Debye-Scherrer method using the diffraction of X-ray beams on powder or micro samples as the planes are oriented equally and this orientation causes 3-D reciprocal space to be projected onto a single dimension. Bragg's law (1912) is used to find the position of peaks by calculating the distance between the parallel planes which is given as,

$$2d.sin\theta = n\lambda \quad \textbf{(iii)}$$

where, d = spacing between adjacent layers,

λ = wavelength of incident X-ray (nm),

Θ = scattering angle (degrees)

n = the order of the diffraction (~1 for the most of the cases)

XRD analysis was done on *PANalytical X'Pert Pro* XRD diffractometer with Cu-Kα radiation, λ=1.5418 Å with an applied voltage of 45 kV, and current range of 40 mA. All the as-synthesized powdered samples were kept in the sample holder and scanned between $20° \leq 2\theta \leq 80°$ with step size of 0.0131° at room temperature. The peak matching of samples was done by matching the cards with International Centre for Diffraction Data (ICDD) [1].

3.2.2 Differential scanning calorimetry/Thermal gravimetric analysis

DSC/TGA helps in analyzing whether the reaction in prepration/decomposition of sample is endothermic or exothermic with rise and fall in temperature [2]. While varying the temperature, there is a change in the physical state of the material, it either release or absorbs heat, which further results in oxidation or reduction of material, thereby having a gain or loss of weight of sample. The analysis were carried out at a heating rate of 5 ºC/min using *NETZSCH STA 449 F3*. The spectrum of the samples 5ZrC700 and 5ZrC800C0.22 was obtained in the temperature range of 30 to 800 ºC under air atmosphere using alumina (Al_2O_3) crucible.

3.2.3 High resolution transmission electron microscopy (HRTEM)

HRTEM is a technique in which an electron beam is transmitted through a very thin sample. The image of these transmitted electrons is magnified and focused onto an imaging device.

The image is then detected with the help of a charge coupled device (CCD). HRTEM provides information about the structural defects, crystal interfaces and the individual grain size with the corresponding lattice spacing [3]. For HRTEM analysis, the powder samples 5ZrC700 and 5ZrC800 C0.22 were dispersed in ethanol after ultra-sonicating them for 30 min to break the agglomeration of nanosized particles. A drop of the solution was deposited on both sides of the carbon coated copper TEM grid and allowed to evaporate at room temperature. The powder samples were analyzed with *JEOL 2100F* instrument and the operating voltage was 200 kV.

3.2.4 UV-Vis spectroscopy

Ultraviolet–visible spectroscopy is the spectroscopy related to absorption or reflectance in the ultraviolet ($\lambda \sim$ 100-400 nm) and visible ($\lambda \sim$ 400-800 nm) region. Due to the absorption or reflectance in the visible range, there is a direct effect on the perceived color of the chemicals. For a given excitation process, a molecule absorbs specific energy, which corresponds to one type of frequency giving rise to an absorption line [4]. However, there is a not a single molecule but a group of them, there are number of vibrational and rotational energy states related to each electronic level so we get a series of absorption peaks. All the samples were tested in *Hitachi U3900H spectrophotometer*. Before the sample testing, the instrument was calibrated for wavelength and zero PMT function, baseline was taken with reference to $BaSO_4$ tablets. The samples were placed in sample holder, rays were passed through it in UV-Vis range, and transmittance (% T) was recorded.

3.2.5 Photocatalytic activity

The photocatalytic activity was analysed for the as-synthesized sample by checking the degradation of methylene blue (MB) dye which is an organic pollutant. The experiment was accomplished in direct sunlight exposure (90000 lux) for a duration of 5h. For this procedure, 0.0001g dye was dissolved in 100ml of distilled H_2O which was stirred for 20 min to make a homogeneous solution. Thereafter, 0.01g of catalyst was added in dye solution. This solution was kept in a dark compartment with continuous stirring for 30 min. This was done to attain the adsorption-desorption equilibrium. The degradation under solar radiation was investigated via *Hitachi U3900H spectrophotometer* at 60 min interval for the duration of 5h.

3.3 References

1. Cullity B.D., ‘‘Elements of X-ray diffraction’’. Addison-Wesley Publishing, London, (1977).
2. P.R. Khangaonkar, An introduction to materials characterization, Penram International Publishing (I) Pvt Ltd, Mumbai, India (2010).
3. Williams D., Carter C., Transmission electron microscopy: A textbook for materials science, Springer, New York (2009).
4. Skoog D., Holler J., Crouch S., Principles of instrumental analysis (6^{th} ed.), Belmont, CA, (2007).

4. Results and Discussion

In order to have better efficiency of the process, the operating temperature (600, 700 and 800 ºC) was varied and different holding times has also been optimized and presented. In the later stages, the carbon content of the sample was also varied to optimize the amount of carbon source. These variations lead to change in crystal-structure, thermal and microstructural features of as-synthesized nano powder which are being discussed in this chapter.

4.1 X-ray diffraction (XRD) analysis

The results of XRD analysis were compared and matched with different standard ICDD cards in *PANalytical X'Pert Highscore Plus* tool to identify the different phases under various synthesis conditions. Almost all the obtained patterns contained 5 diffraction peaks of ZrC corresponding to (111), (220), (200), (311) and (222) planes respectively which asserted NaCl type structure of space group fm-3m [1]. The standard cards from which peaks were matched are enlisted below:

Table 4.1: List of standard ICDD cards used in proposed work.

S. No.	ICDD card	Phase	Crystal structure
1.	03-065-0332	ZrC	FCC
2.	01-074-0815	ZrO_2	Monoclinic
3.	01-089-7710	ZrO_2	Tetragonal
4.	00-026-1080	C	HCP

The information from the XRD peaks was extracted by measuring peak positions and β_{hkl} which is full width at half maxima by means of Pearson's VII fitting of peak profile. Lattice constant 'a' (defined as a physical dimension of unit cell in a crystal lattice) was calculated using Bragg's diffraction law by calculating the interplanar spacing d_{hkl} from the following formulae,

$$\boldsymbol{d_{hkl} = \frac{n\lambda}{2\,sin\theta_{hkl}}} \qquad \text{and} \qquad \boldsymbol{a = d\sqrt{h^2 + k^2 + l^2}} \qquad \textbf{(iv)}$$

which is in tune with the standard value of 4.6941 Å (ICDD 03-065-0332).

4.1.1 Effect of temperature on the synthesis of ZrC

ZrC was synthesized at different temperatures (600 and 700 °C) and the corresponding XRD data was recorded which is shown in figure 4.1. It can be seen from the XRD patterns that the synthesis conditions including temperature and holding time play vital role in preparation of ZrC. As a Zr source, ZrO_2 was taken and through XRD spectra, it was determined that ZrO_2 powder was a mixture of m-ZrO_2 (monoclinic) and t-ZrO_2 (tetragonal) as shown in figure 4.1a. In the beginning, when the sample was heated at 600 °C for 5 and 10h the reduction and carburization could not occur as is evident from fig. 4.1 (b & c) where all the peaks corresponds to m-ZrO_2 (stable at low temperature) and t-ZrO_2 phases [2]. However, when the sample was heated to 700 °C for 5h simultaneous reduction-carburization process was observed resulting single phase spectrum of ZrC (figure 4.1 d). The broad peaks corresponds to nano ZrC but were highly strained (discussed later). To reduce it and also to introduce higher crystallanity, heating time was increased to 10h, apart from ZrC peak, peak of carbon (at $2\theta = 26°$) was also obtained. Such a transformation of carbon in longer holding time might be associated to the graphitization of extra amorphous carbon which was not visible in 5ZrC700 [3]. This is because of the fact that graphitic C around ZrC particles has been on higher side and moreover, some excess C has also been converted to graphitic carbon.

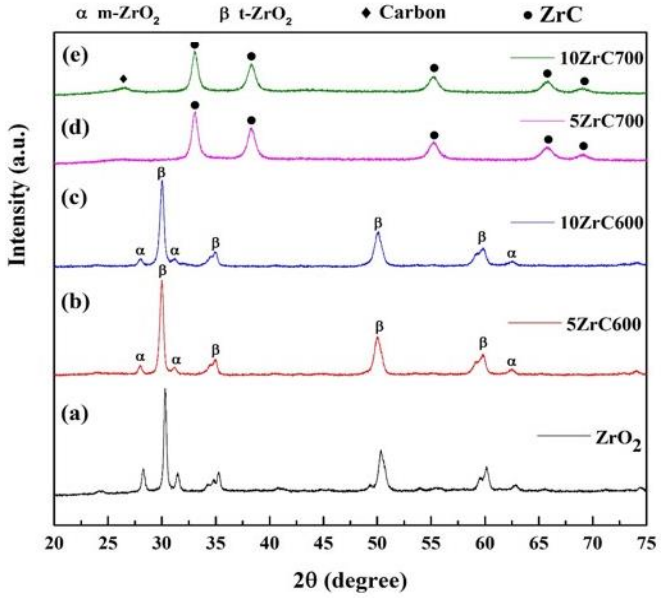

Figure 4.1: Effect of synthesis temperature on the developed phases during the formation of ZrC.

It may also be noted that at lower temperature (600 °C), the reaction didn't have sufficient thermal energy to reduce ZrO_2 completely which is associated to broadened peak along with shifting towards lower angle. It can be accomplished that reduction-carburization reaction mechanism at different temperatures affects the formation of crystallite in Zr unit cell by the movement of C and O_2 atoms. Though, pure phase is observed in 5ZrC700, but at this temperature amorphous C was present and when holding time was increased to 10h (10ZrC700) amorphous carbon changed to graphitic C which is attributed to the fact that at higher temperatures graphitization takes place in which amorphous C transforms to graphitic C which is clearly visible in the XRD pattern (figure 4.2 e) [4]. However, peak intensities indicate that complete transformation of amorphous C to graphitic C has not taken place, thus, the optimization of process variables to get ZrC at 800 °C was done by varying the holding time and afterwards by varying carbon content which is presented in subsequent sections.

4.1.2 Effect of variation of holding time at 800 °C on the synthesis of ZrC

As per the earlier discussions, after the optimization of the synthesis conditions pure ZrC was obtained at 700 °C at 5h of holding time. In this particular section, effect of impregnation time is investigated at different time durations (2.5h, 5h, 7h and 10h) at 800 °C. Figure 4.2 shows the effect of holding time on the as-synthesized sample. The amount of graphitic carbon has been decreased as the holding time is reduced from 10ZrC800 to 2.5ZrC800 asserting the time dependency of graphitization at constant temperature.

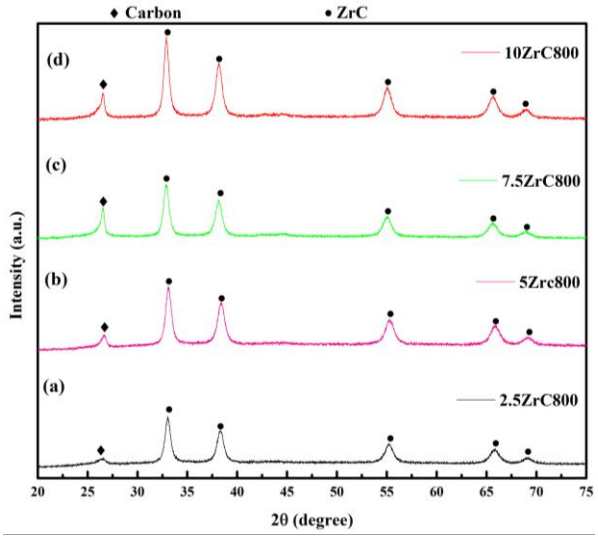

Figure 4.2: Effect of holding time at 800 °C on the synthesis of ZrC.

Also, at different holding times variation in lattice parameters was observed, which is shown in figure 4.3 and given in table 4.3. It is observed that reaction parameters also affect the lattice parameters of ZrC; first it decreases upto 5h then increases when holding is further decreased to 2.5h which may be attributed to diffusion of C in ZrC. As observed from XRD data, carbon needs to be diffused into Zr lattice to from ZrC which is not getting fulfilled resulting to the stretching of unit cell. While, 5h holding at 800°C is assumed as the optimized condition for the occupancy of carbon in its equilibrium position in Zr lattice to form FCC unit cell of ZrC. The deviation from standard lattice parameter is least in the case of 5ZrC800, therefore the amount of hexane is optimized keeping the same operating conditions as 5ZrC800.

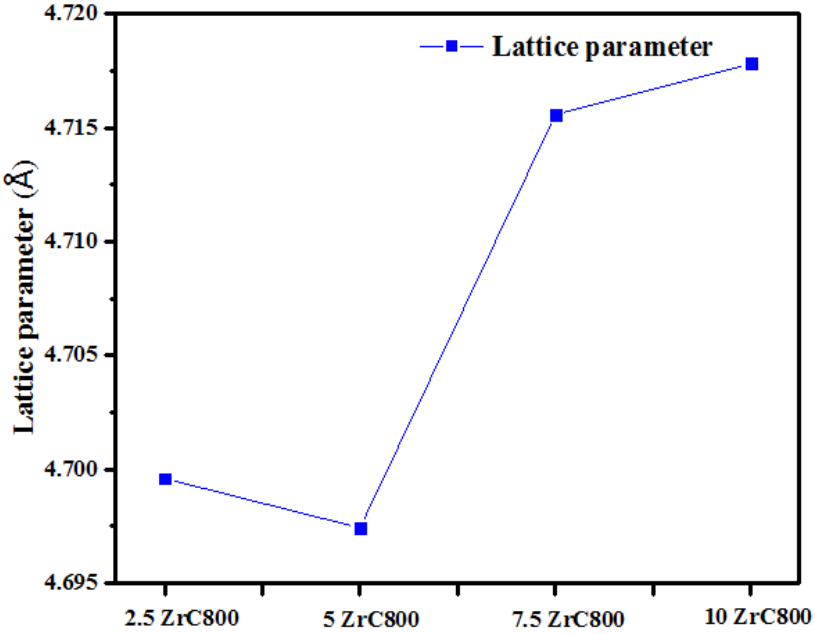

Figure 4.3: Variation of lattice parameter at different holding time at 800 °C.

4.1.3 Effect of variation of carbon content at 800 °C on the synthesis of ZrC

After synthesizing ZrC at various temperatures and holding times, 5h holding time at 800 °C was chosen to study the effect of variable amount of C-source. The proposed reaction for the synthesis of ZrC is given as follows:

$$6ZrO_2 + C_6H_{14} + 5Mg \rightarrow 6ZrC + 5MgO + 7H_2O \quad \textbf{(v)}$$

In the above equation (v), going by the stoichiometric norms, molar ratio 6:1:5 was taken of ZrO_2, hexane and magnesium respectively. All the above samples were synthesized with 0.01 moles of ZrO_2 and 0.45 moles of C_6H_{14} (10 ml). Such a high amount of C_6H_{14} was taken deliberately to generate higher partial pressure inside the autoclave. To have an indirect idea of partial pressure, different molar concentrations of C_6H_{14} were used for reaction in autoclave. The crystallographic data was observed via XRD pattern which is shown in figure 4.4. It is clear that the C peak intensity decreases as we go on decreasing the amount of C and diminishes completely when the stoichiometry (1:1) and sub-stoichiometry (1:0.9) was maintained.

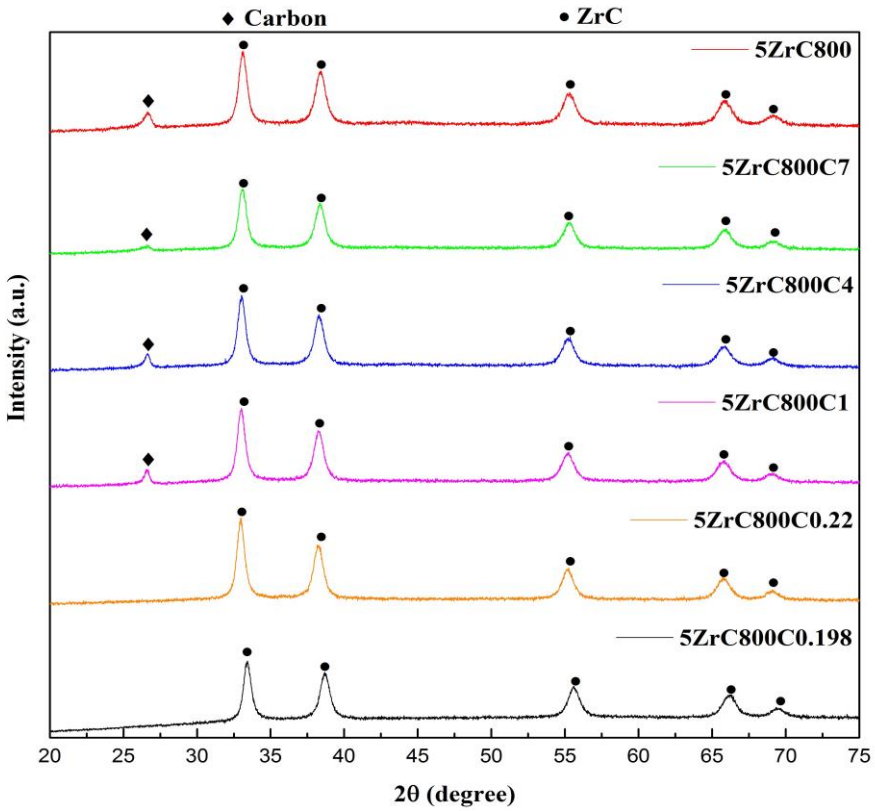

Figure 4.4: Variation of carbon content at 5h holding at 800 °C.

The variation of lattice parameter (a) with the variation of the C content is shown in figure 4.5. In 5ZrC800, a = 4.6974 Å. However, on decreasing the carbon content, 'a' decreases upto 7ml of precursor content which can be attributed to profused layer of C on ZrC which stops the C to diffuse into ZrC then keeps on increasing upto 0.22ml due to sufficient concentration required for C to diffuse in ZrC. Also a drastic jump is seen as C content is

changed to 0.9 mole from 1 mole which is related to the insufficient amount of carbon used for the reaction. The superscripts in the graph represents the number of moles of C taken.

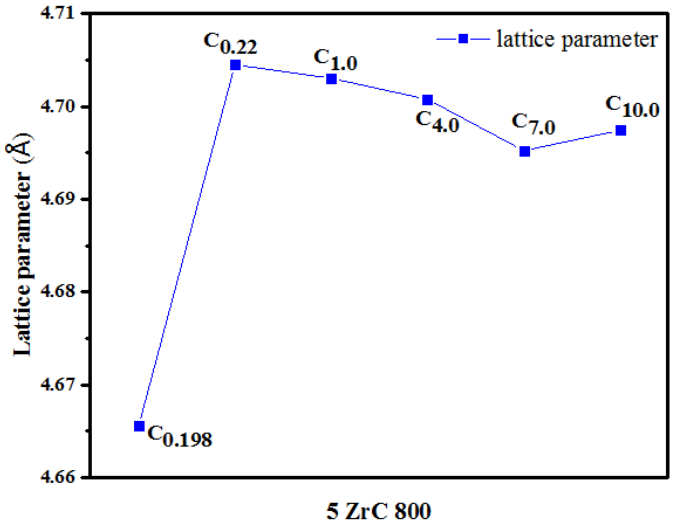

Figure 4.5: Variation of lattice parameter with varying carbon content at 800 °C.

4.2 Williamson – Hall analysis

XRD is considered to be one of the most versatile techniques for calculation of particle size, lattice parameter and much more. One of the methods used to calculate the crystal size is Scherrer method. It relates to the size of the particles to the broadening of the peak in a diffraction pattern and was given by Paul Scherrer in 1918 [5] and is given as,

$$t = \frac{k\lambda}{\beta_{hkl}\, cos\theta_{hkl}} \qquad \textbf{(vi)}$$

where, k is the shape factor value of which is taken to be almost equal to 1, θ is Bragg's angle and wavelength, λ = 0.15406 nm. The broadening of strain is given by Stokes and Wilson formula [6]. As per their calculations, ε which is the induced strain is written as:

$$\beta = 4.\varepsilon.tan\theta_{hkl} \qquad \textbf{(vii)}$$

As per the Williamson-Hall plot the FWHM is the combination of both equation (vi) and (vii) which is given as:

$$\beta_{hkl}\, cos\theta_{hkl} = \frac{k\lambda}{t} + 4.\varepsilon.sin\theta_{hkl} \qquad \textbf{(viii)}$$

The above equation represents the USM model of W-H analysis which is based on the fact that distribution of strain is isotropic in the whole crystal. By drawing a graph between $\beta_{hkl}\cos\theta_{hkl}$ vs $4\sin\theta_{hkl}$, we can find the slope and intercept through which the strain and size of the particle respectively can be calculated [7]. β_{hkl} mainly depends on tanθ instead of

being depending on $(\cos\theta)^{-1}$, as a result of which the diffracted beams can be separated easily when crystallite size and strain are involved concurrently [8]. The samples were fitted with Pearson VII curve fitting via Origin 2016 software and some of the curve fittings is shown below.

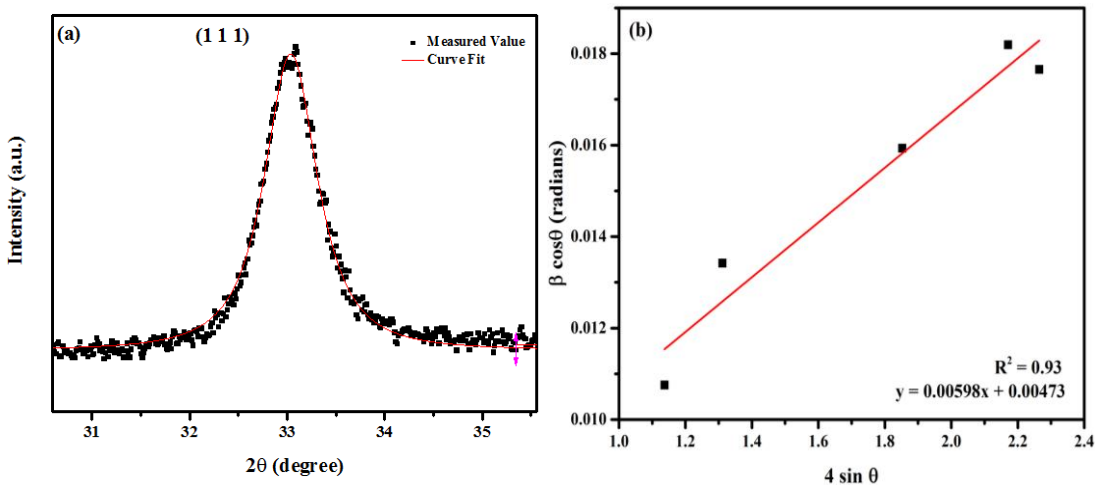

Figure 4.6: The W-H analysis of the sample '5ZrC700', the crystalline size is extracted from the y-intercept of the fit. The strain and stress is extracted from the slope (a) Pearson VI fitted data, (b) USM.

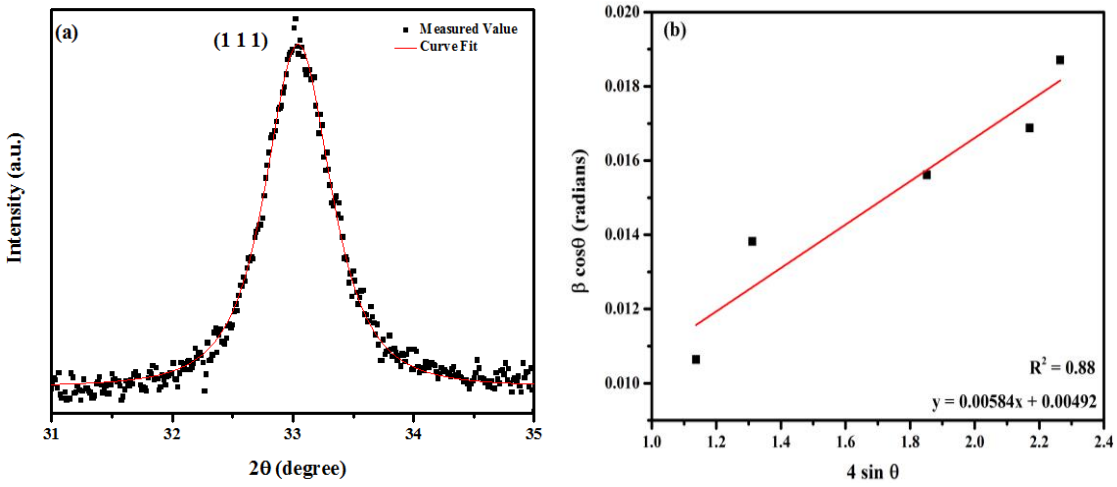

Figure 4.7: The W-H analysis of the sample '10ZrC700', the crystalline size is extracted from the y-intercept of the fit. The strain and stress is extracted from the slope (a) Pearson VII fitted data, (b) USM.

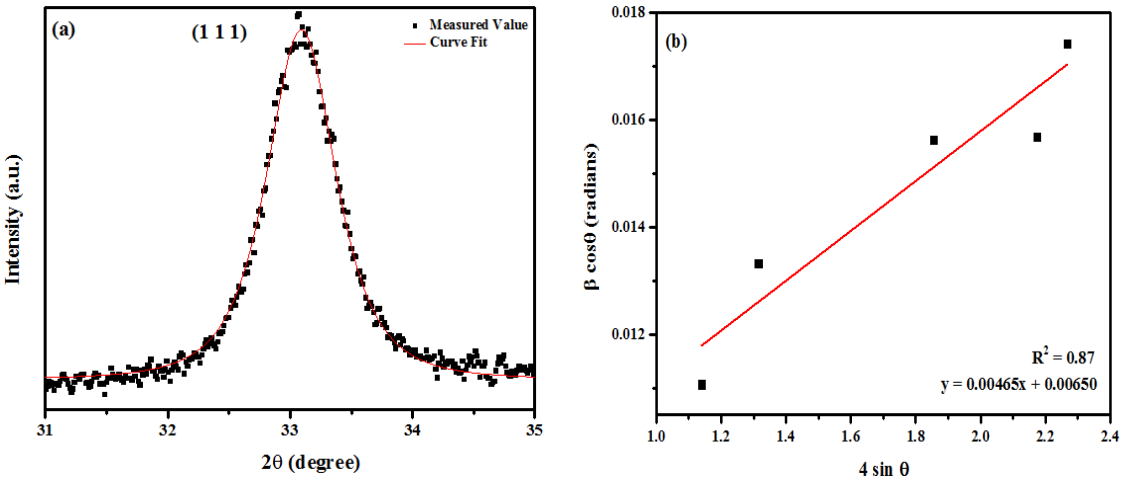

Figure 4.8: The W-H analysis of the sample '5ZrC800', the crystalline size is extracted from y-intercept of the fit. The strain and stress is extracted from the slope (a) Pearson VII fitted data, (b) USM.

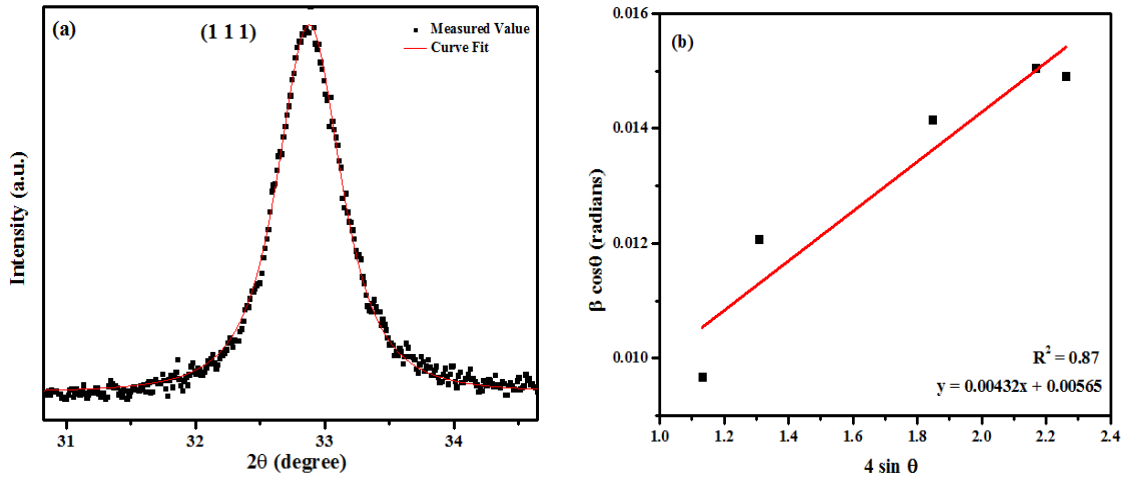

Figure 4.9: The W-H analysis of the sample '10ZrC800', the crystalline size is extracted from the y-intercept of the fit. The strain and stress is extracted from the slope (a) Pearson VII fitted data, (b) USM.

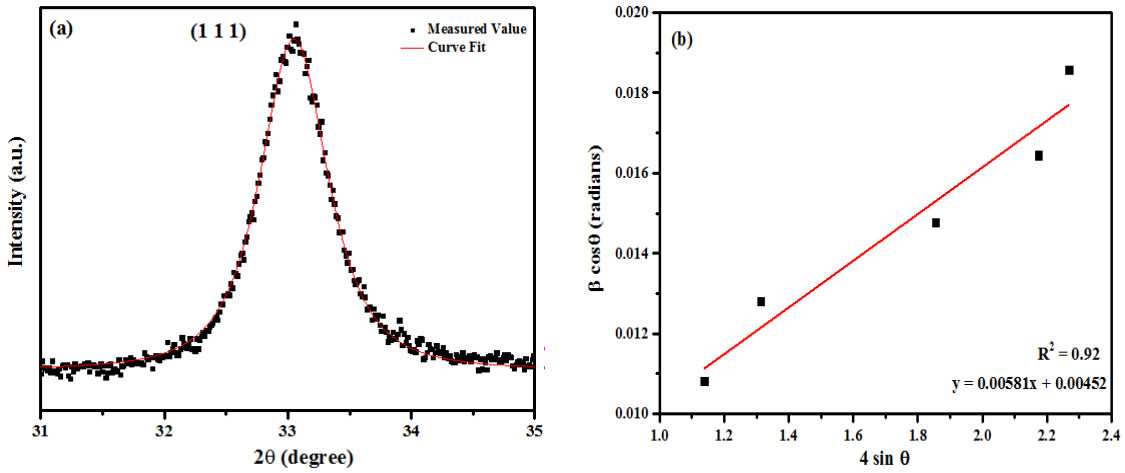

Figure 4.10: The W-H analysis of the sample '2.5ZrC800', the crystalline size is extracted from the y-intercept of the fit. The strain and stress is extracted from the slope (a) Pearson VII fitted data, (b) USM.

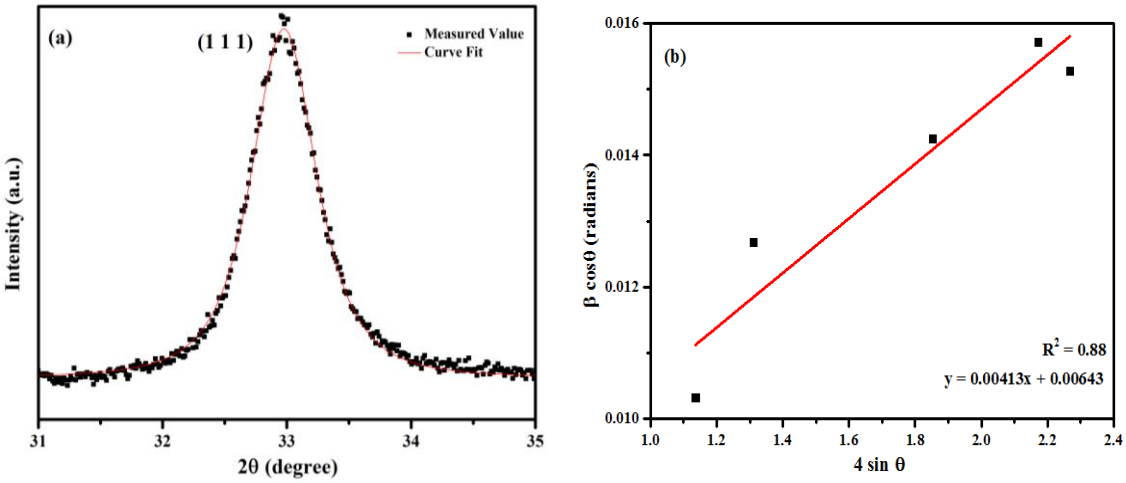

Figure 4.11: The W-H analysis of the sample '5ZrC800 C0.22', the crystalline size is extracted from the y-intercept of the fit. The strain and stress is extracted from the slope (a) Pearson VII fitted data, (b) USM.

The table 4.2 shows the Williamson – Hall analysis of all the synthesized ZrC samples and the amount of strain calculated from the USM model along with the particle size calculated from the Scherrer method. From the table 4.2, it can be seen 5ZrC700 contains maximum strain i.e. 5.98, while if we go towards higher temperature 800 °C the induced strain is less which is also confirmed by the peak broadening of 5ZrC800. The peaks grow narrower and more intense as we go towards 10ZrC800. On varying the holding time, the value of strain increases as the holding time is reduced with an exception of 5ZrC800 which has a less value of 4.65 as it shows the least deviation from the standard lattice parameter. The highest

particle size is of the sample with the least amount of holding time at 2.5h. If we go by variation of hexane, the amount of strain keeps on decreasing and is least when the stoichiometry of C to Zr is 1:1. Intensity of peaks of carbon also decreases simultaneously as is clearly shown in fig. 4.4.

Table 4.2: Williamson – Hall analysis of each of the synthesized samples.

Sample ID	USM		Scherrer Method, t(nm)
	$\epsilon \times 10^{-3}$	t (nm)	
5ZrC700	5.98	30.59	9.89
10ZrC700	5.84	29.41	9.93
2.5ZrC800	5.81	32.01	10.21
5ZrC800	4.65	22.26	10.14
7.5ZrC800	5.60	29.96	10.27
10ZrC800	4.32	25.61	11.29
5ZrC800 C7	4.34	22.33	10.50
5ZrC800 C4	5.16	27.15	10.40
5ZrC800 C1	4.80	24.73	10.45
5ZrC800 C0.22	4.13	22.50	10.85
5ZrC800 C0.198	4.17	22.93	10.84

Table 4.3: List of d-spacing and lattice constants of synthesized samples.

Sample Id	Interplanar spacing 'd' (111) (nm)	Lattice Constant (Å)
5ZrC600	-	-
10ZrC600	-	-
5ZrC700	0.27097	4.7039
10ZrC700	0.27093	4.7042
2.5ZrC800	0.27088	4.6996
5ZrC800	0.27055	4.6974
7.5ZrC800	0.27215	4.7155
10ZrC800	0.27224	4.7178
5ZrC800 C7	0.27052	4.6952
5ZrC800 C4	0.27099	4.7007
5ZrC800 C1	0.27119	4.7030
5ZrC800 C0.22	0.27146	4.7044
5ZrC800 C0.198	0.26789	4.6656

The list of as-synthesized samples along with their lattice parameter (a) and corresponding interplanar spacing (d) is given in table 4.3. From the table, it can be seen that as the holding time is increased at 700 °C (5ZrC700 & 10 ZrC700) the lattice constant increased. This is true for samples synthesized at 800 °C wherein any increase in holding time leads to increase in lattice constant 'a'. This increase in 'a' may be attributed to the fact that the formation of ZrC, which is a multistep reduction-carburization is a fast process, resulting in fast diffusion rate of C. So, the carbon which is being diffused in the crystallites either is not getting the sufficient time for diffusion or else it is being diffused in non-optimal locations [8]. On the other hand, on decreasing the amount of hexane in the sample, the behavior of 'a' changes, its value is less for C = 10ml and 7ml which might be due to the thickness of graphitic C on the ZrC boundaries causing hindrance in the diffusion of C in ZrC. With decrease in C content, 'a' increases as the concentration gradient is sufficient for the diffusion of C in ZrC particles. Further, decrease in C content results in abrupt change in the value of 'a' which may be due to the insufficient C present in the sample.

4.3Thermal analysis

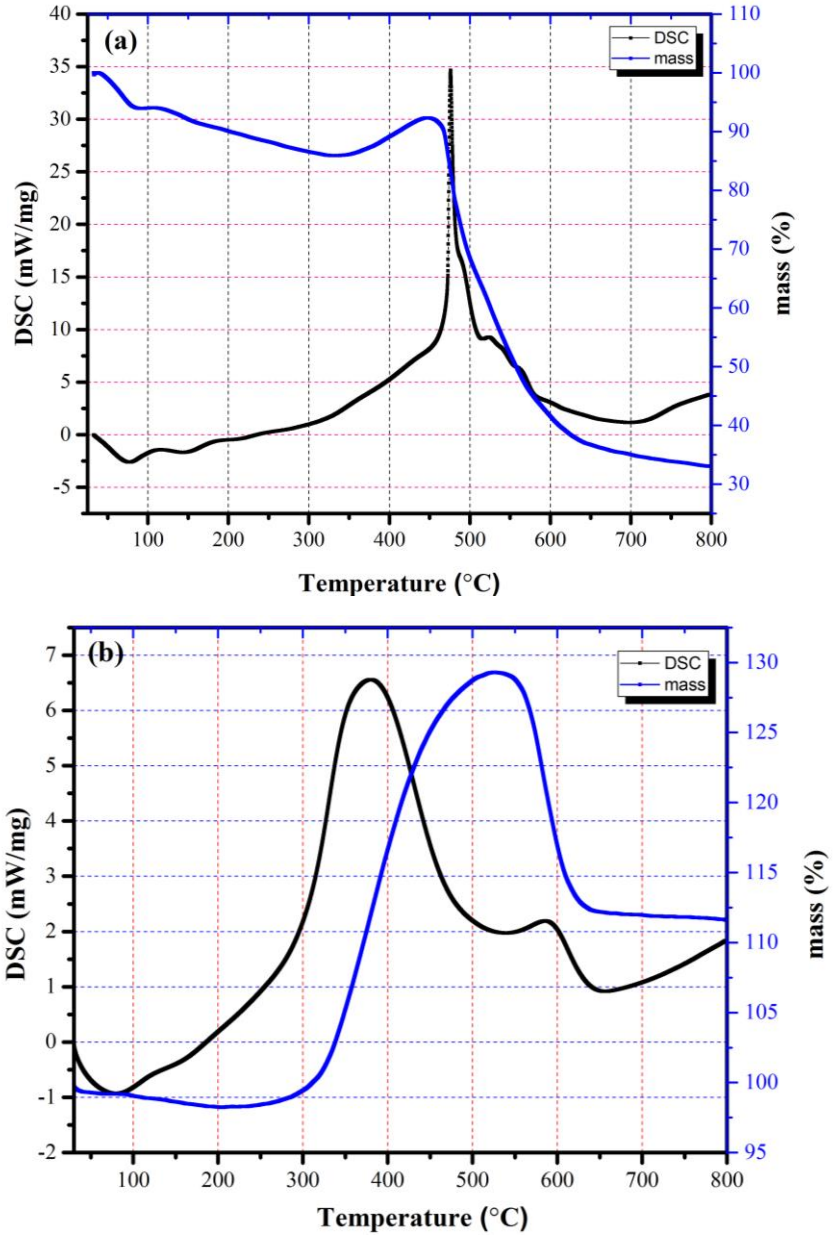

Figure 4.12: DSC/TGA study of (a) 5ZrC700 and (b) 5ZrC800 C0.22.

Samples '5ZrC700' and '5ZrC800 C0.22' were subjected to study the thermal stability in air atmosphere via DSC/TGA analysis which is shown in fig.4.12. From XRD analysis it was clear that both the samples have single phase spectra in spite of different amount of hexane which is very clear in TGA graph of both the samples. Both the samples showed slight weight loss of 13% and 5% respectively upto 300 °C which might be associated to

the loss of adsorbed water and surface contaminations. Beyond 300 °C, both the samples behave differently due to presence of different amounts of C. In region 350-450 ºC, small weight gain of 6.7% is observed in the sample 5ZrC700 which corresponds to adsorption of O_2 on powder sample resulting in the oxidation of ZrC particle [10,11]. While, 5ZrC800 C0.22 showed a significant weight gain of around 24% which is caused by the transformation of ZrC to ZrO_2 following the chemical reaction mentioned as follows [10]:

$$\boldsymbol{O_2 + ZrC \rightarrow ZrO_2 + C} \qquad \textbf{(ix)}$$

It is a very well-known fact that beyond 450 °C, free carbon has a tendency to evaporate, resulting in formation of CO or CO_2 which is clearly illustrated in both the samples as a significant weight loss of 60% is observed in 5ZrC700 upto 630 °C [12]. With further increase in temperature ZrO_2 was formed slowly upto 800ºC indicating that O_2 has the tendency to diffuse at high temperatures to attain a stable phase configuration [13]. With further increase in temperature, the rate of diffusion of O_2 atoms through layer of ZrO_2 will increase [14]. After converting from ZrC to ZrO_2 at 630 °C the sample becomes stable till 800 °C. According to Maitre *et al.* [15] ZrC has the potential for high-temperature structural applications because of the low surface energy. From the graph it can be concluded that the sample has good thermal stability below 300 °C.

4.4 Microstructural analysis

The HRTEM analysis of the sample 5ZrC700 and 5ZrC800 C0.22 shows the agglomeration of nano particles which is clearly shown in figure 4.13 a & b respectively.

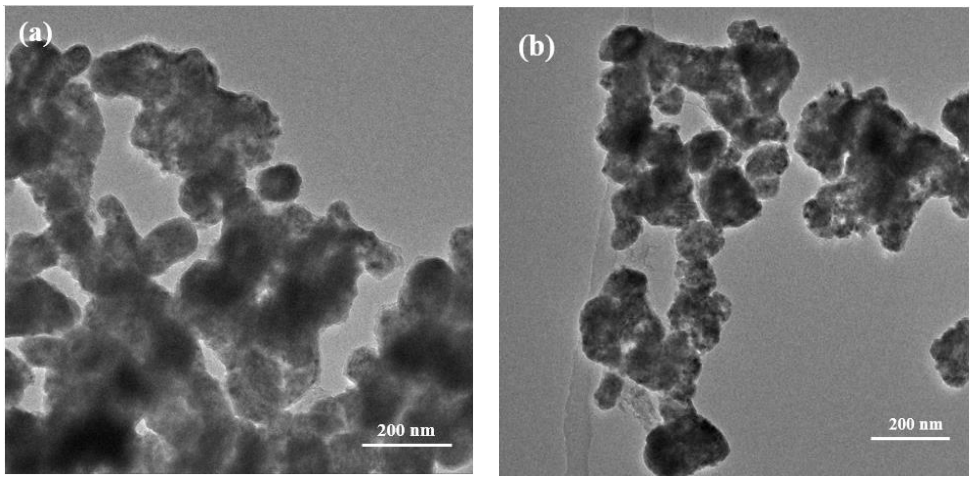

Figure 4.13: (a) HRTEM micrograph showing morphological features of sample 5ZrC700, (b) HRTEM micrograph of 5ZrC800 C0.22 having agglomerated morphology.

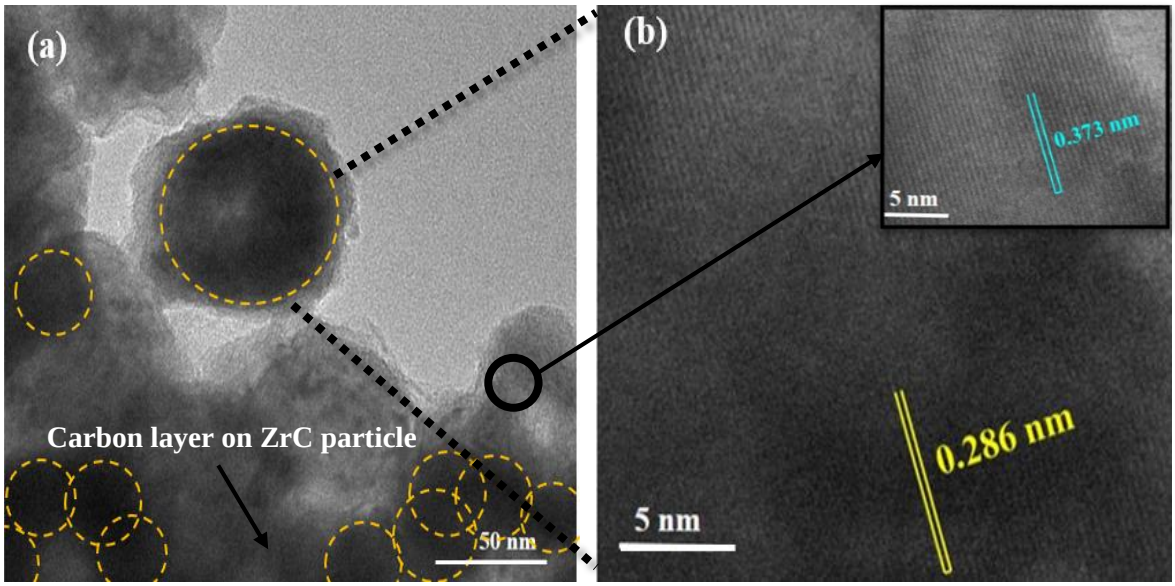

Figure 4.14: (a) HRTEM micrograph of sample 5ZrC700 indicating the carbon layer on ZrC particle, (b) lattice fringes of plane (200) of cubic ZrC.

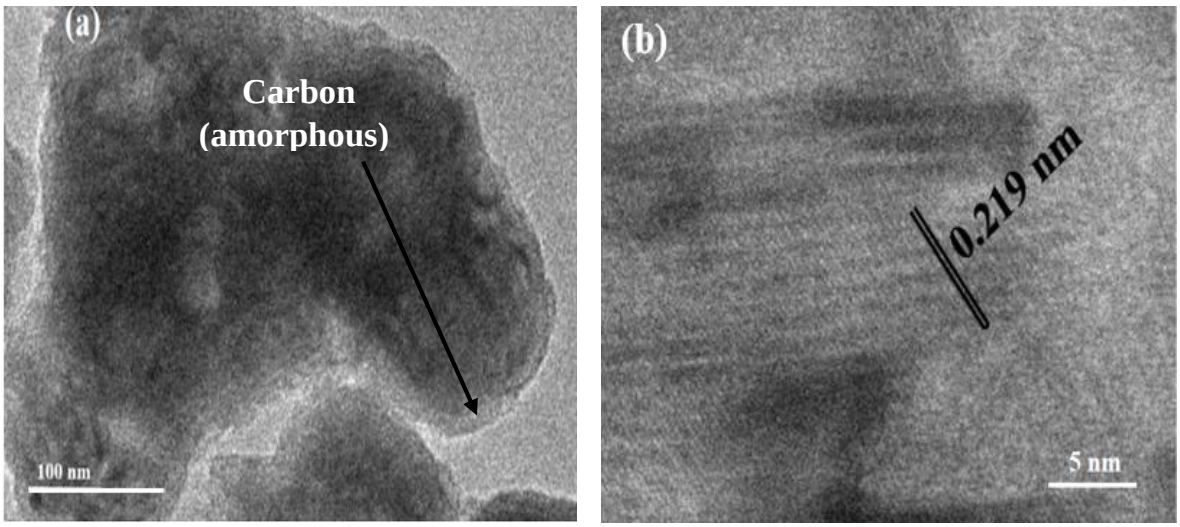

Figure 4.15: (a) HRTEM micrograph of sample '5ZrC800 C0.22' indicating the carbon layer on ZrC particle, (b) lattice fringes of plane (111) of cubic ZrC.

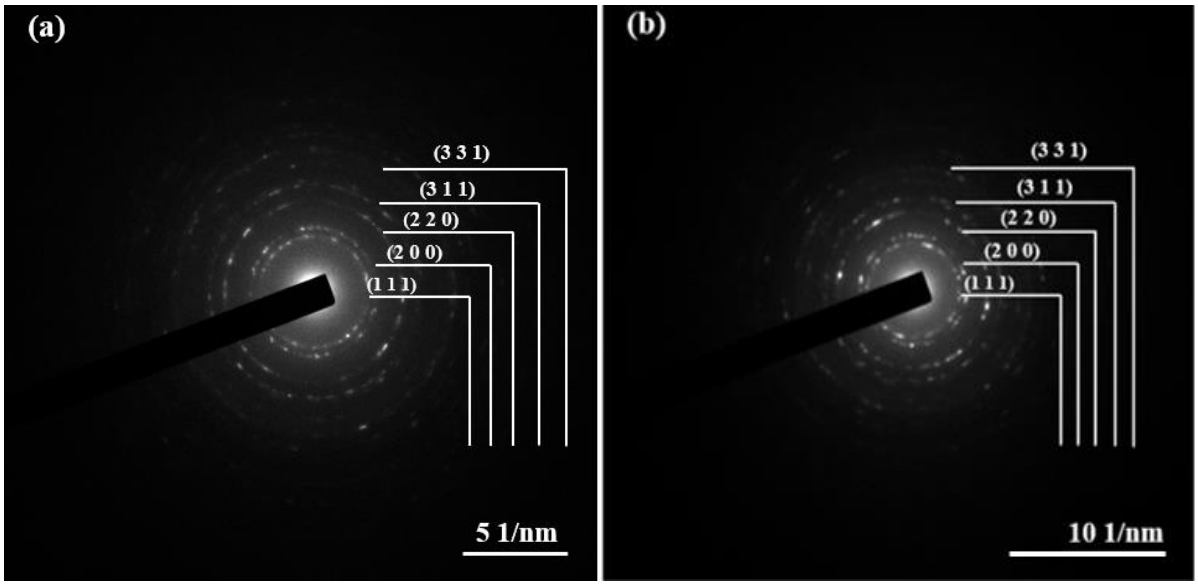

Figure 4.16: SAED pattern micrograph of sample (a) 5ZrC700 (b) 5ZrC800 C0.22 of cubic ZrC.

Fig. 4.14a shows the TEM micrograph of the sample 5ZrC700 in which a layer of amorphous C is adsorbed on ZrC particle surface in the form of floccules which is associated to the high content of the hexane used to synthesize ZrC at 700 °C. Fig. 4.14b shows the lattice fringes of the sample 5ZrC700 which are equivalent to 0.286nm and 0.373nm which corresponds to the (200) plane of ZrC and (004) plane of C respectively. TEM analysis of '5ZrC800 C0.22' shown in figure 4.15a shows the coated morphology of ZrC particle and it can also be confirmed from the figure that on shrinking the C content to the stoichiometric ratio the thickness of C layer also diminishes. Fig. 4.15b shows the lattice fringes which corresponds to (111) plane having an interplanar spacing value (d) of 0.219 nm. In combination with the HRTEM images, the selected area electron diffraction (SAED) patterns of both the samples 5ZrC700 and 5ZrC800 C0.22 which can be seen in fig. 16a and 16b respectively shows that the particles have diffused ring structure clearly visible in the micrographs which further confirms the formation of ZrC having polycrystalline nature. Also, the structure of the synthesized particles are agglomerated and interface is not distinct which further suggests their transient nature.

4.5 Optical analysis

Optical properties of the various ZrC samples were investigated by UV-Vis spectroscopy as shown in below figures. Figures 4.17a and 4.18a, shows the absorption of UV-Vis rays in the range 300-650 nm suggesting the broad absorption spectrum of synthesized samples is in the visible region.

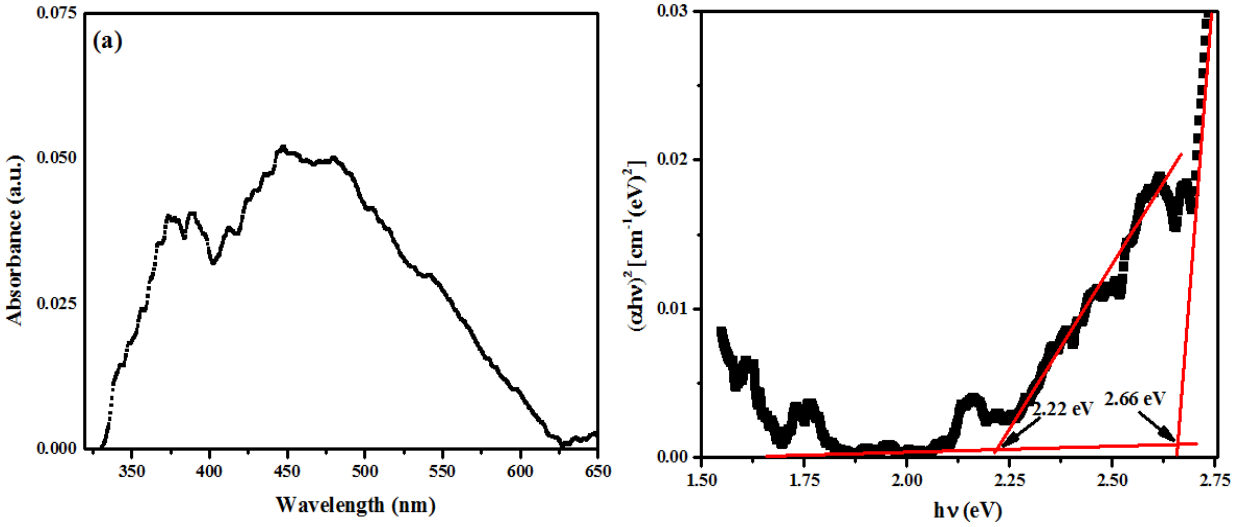

Figure 4.17: (a) Absorption spectra of sample 5ZrC700 in the range 300-650 nm, (b) Tauc plot of 5ZrC700 with band gaps of 2.22 eV and 2.66 eV.

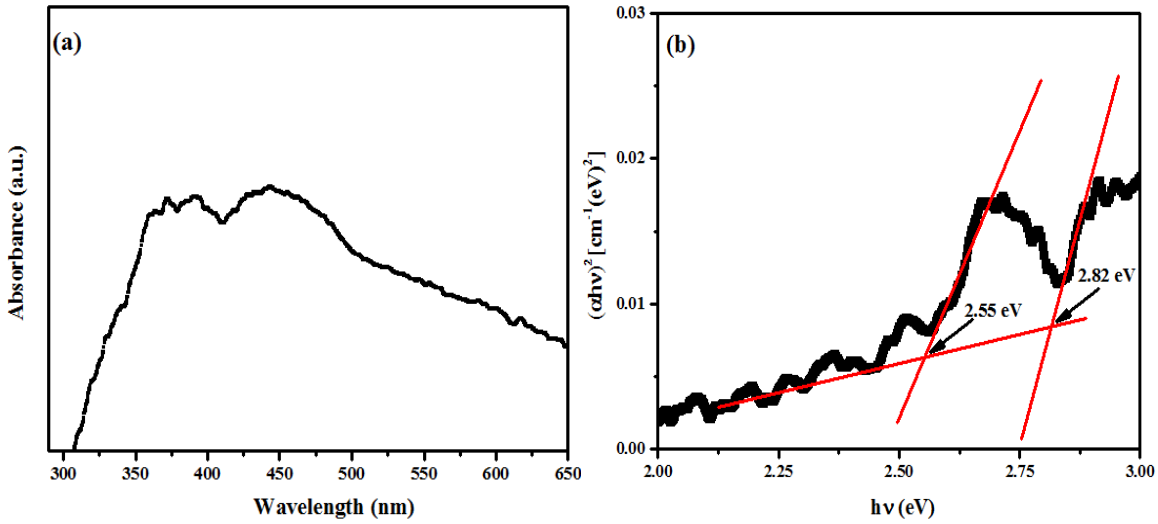

Figure 4.18: (a) Absorption spectra of sample 5ZrC800 C0.22 in the range 300-650 nm, (b) Tauc plot of 5ZrC800 C0.22 with band gaps of 2.55 eV and 2.82 eV.

Figure 4.17a and 4.18a of sample 5ZrC700 and 5ZrC800 C0.22 respectively reveals a broad absorption band in near UV-region. The center of maxima lies at ~ 448.2 nm and

442.3 nm, which are associated with the n-π* transition of C = O bonds [17]. Tauc plot is used to calculate the optical band gap in case of semiconductors. The Tauc gap is often used to characterize the optical properties of amorphous materials and is generally plotted between hυ vs $(\alpha h\upsilon)^{1/r}$ where r denotes the nature of transition. The band gap is calculated by using the modified form of Tauc plot [18,19]:

$$\boldsymbol{\alpha h\upsilon = A(h\upsilon - E_g)^n} \qquad \textbf{(x)}$$

where 'A' is constant, 'α' is the absorption coefficient and 'n' corresponds to various transition levels with values 1/2 (allowed direct), 2 (allowed indirect), 3/2 (forbidden direct) and 3 (forbidden indirect) [20]. As ZrC is an indirect band-gap semiconductor so n is taken to be 2. By the extrapolation of the straight line portion of the graph between $(\alpha h\upsilon)^2$ vs hυ the exact value of band gap was obtained. In the present work, the band gaps are calculated from the Planck's radiation formula given in equations xi (i) and (ii):

$$\boldsymbol{E = {hc}/{\lambda}} \qquad \textbf{xi (i)}$$

$$\boldsymbol{E = {1244}/{\lambda(nm)}} \qquad \textbf{xi (ii)}$$

where, $Planck's\ constant, h = 6.626 \times 10^{-34}\ m^2$ kg/s and $c = 3 \times 10^8\ m/s$

The band gaps were found to be 2.22 (560.36 nm) and 2.66 eV (448.2 nm) corresponding to 5ZrC700. Also, 2.55 eV (487.84 nm) and 2.82 eV (442.3 nm) corresponding to 5ZrC800 C0.22 (fig. 23b and 24b). Due to this, it is expected to possess large breakdown field. This value of band gap comes under indirect wide band gap semi-conducting materials [21], and is used for high temperature applications [22].

4.6 Photocatalytic activity

The degradation of methylene blue (MB) dye was investigated by as- synthesized sample 5ZrC800 C0.22. Figure 25(a) shows the calibration curve of MB (black curve) and various concentration of MB at different time interval. As a result of adsorption-desorption equilibrium, 26.15 % dye has been adsorbed on the surface of ZrC nanoparticles after 30 min as shown in figure 25b. Further, the exposure of solar irradiations over solution resulted to the photodegradation of MB dye in the presence of as-synthesized photocatalyst as shown in figure 25b. Moreover, the efficiency of the degradation of MB can be calculated from the given eqaution [23]:

$$D(\%) = \frac{C_o - C_t}{C_o} \times 100 \qquad \textbf{(xi)}$$

where, C_o and C_t represent the concentration of the dye at time t = 0 and t = t, respectively. After the exposure of 5h, 80.21% dye was degraded which may be associated to the generation of electrons and holes responsible for the formation of hydroxyl radical ($\dot{O}H$) and super oxide anion radical ($\dot{O_2^-}$) to degrade MB molecule [20].

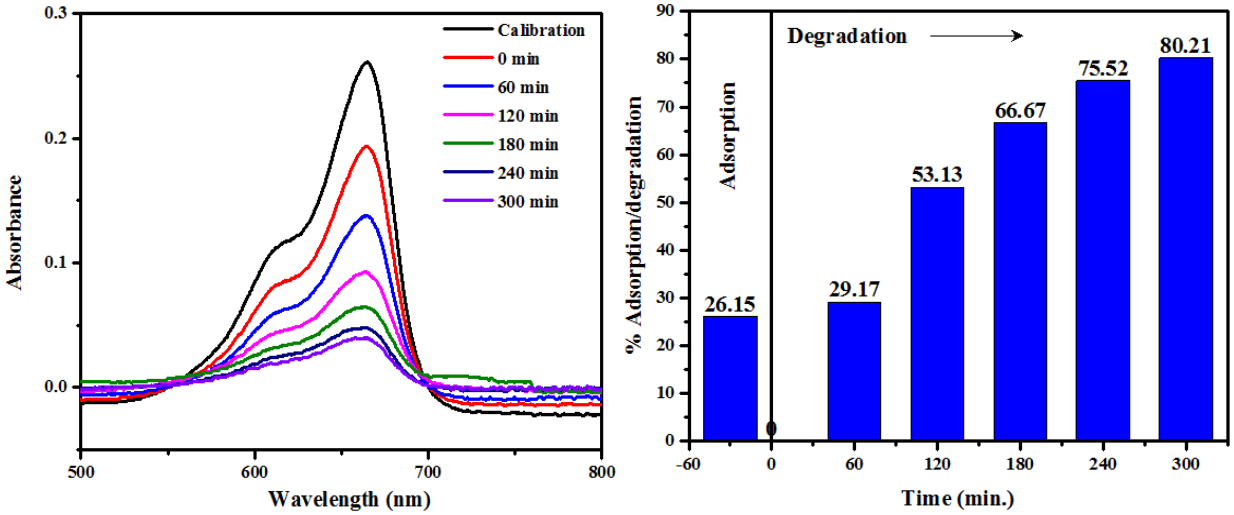

Figure 4.19: (a) Absorption spectra of MB dye at various exposure intervals. (b) %age degradation of 5ZrC800 C0.22 at different intervals of time.

4.7 References

1. Lawson A., Butt D., Richardson J., Li J., Thermal expansion and atomic vibrations of zirconium carbide to 1600 k, Philos. Mag. 87 (2007) 2507–2519.
2. Mahdavi M., Ramazani M., Darvishi Z., Synthesis and characterization of zirconium carbide nanorods at low temperature, Int. J. Refract. Met. Hard Mater.56 (2016) 59-62.
3. Han F., Yao B., Bai Y., Preparation of carbon nano-onions and their application as anode materials for rechargeable lithium-ion batteries, Phys. Chem. C 115 (18) (2011) 8923–8927.
4. Barbera K., Frusteri L., Italiano G., Spadro L., Frusteri F., Perathiner S., Centi G., Low-temperature graphitization of amorphous carbon nanospheres, Chinese Journal of Catalysis 35 (6) (2014) 869-876.
5. Scherrer P., Bestimmung der Grösse und der inneren Struktur von Kolloidteilchen mittels Röntgenstrahlen, Nachr. Ges. Wiss. Göttingen, 26 (1918) 98-100.
6. Vives S, Gaffet E., Meunier C., X-ray diffraction line profile analysis of iron ball milled powders, Mat. Sci. and Eng. A 366(2) (2004) 229-238.
7. Singla G., Singh K., Pandey O.P., Willianson-Hall study on synthesized nanocrystalline tungsten carbide (WC), Applied Physics A, 113(1) (2013) 237-242.
8. Brar L., Singla G., Pandey O.P. Role of carbon in structural evolution during single step synthesis of nano tantalum carbide, RSC Adv. 6 (2016) 109174-109184.
9. Zak A., Majid W., Abrishami M., Yousefi R., X-ray analysis of ZnO nanoparticles by Williamson-Hall and size-strain plot methods, Solid State Sciences 13(1) (2011) 251.
10. Da A., Long F., Wang J., Preparation of nano-sized zirconium carbide powders through a novel active dilution self-propagating high temperature synthesis method, J. Wuhan Univ. Technol. Sci. Ed. 30(4) (2015) 729-734.
11. Gupta A., Singla G., Pandey O.P., Effect of synthesis parameters on structural and thermal properties of NbC-C nano composite synthesized via in-situ carburization reduction route at low temperature, Ceramics Int. 42 (11) (2016) 13024-13034.
12. Zhilyaev V., Zainulin Yu., Alyamovskii S., Shveikin G., High-temperature oxidation of zirconium and hafnium oxycarbides, and oxycarbonitrides, Soviet Powder Metallurgy and Metal Ceramics 11(8) (1970) 632-636.

13. Shevchenko A., Lyutikov R., Andrievskii R., Terekhova V., Oxidation of zirconium and niobium carbides, Soviet Pow. Met. and Metal Cer. 19(1) (1980) 48-52.
14. Wang L., Si L., Zhu Y., Qian Y., Solid-state reaction synthesis of ZrC from zirconium oxide at low temperature, Int. J. Refract. Met. Hard Mater. 38 (2013) 134-136.
15. Maitre A., Lefor P., Solid state reaction of zirconia with carbon. Solid State Ionics.104 (1997) 109-122.
16. Mahajan M., Lalla N., Singh K., Pandey O.P., Synthesis and photoluminescence properties of in-situ synthesized core shell (m-VC@C) nanocomposites, Materials Chemistry and Physics 160 (2015) 1-11.
17. Wen X., Yu P., Toh Y., Lee Yu., Huang K., Huang S., Shrestha S., Conibeer G., Tang J., Ultrafast electron transfer in the nanocomposite of the graphene oxide–Au nanocluster with graphene oxide as a donor, J. Mater. Chem. C 2 (2014) 3826-3834.
18. Murphy A., Band-gap determination from diffuse reflectance measurements of semiconductor films, and application to photoelectrochemical water-splitting, Sol. Energ. Mat. Sol. Cells 91 (2007) 1326–1337.
19. Tauc J., Grigorovici R., Vancu A., Optical properties and electronic structure of amorphous germanium, Phys. stat. sol. 15 (1966) 627-637.
20. Mittal M., Sharma M., Pandey O.P., UV–Visible light induced photocatalytic studies of Cu doped ZnO nanoparticles prepared by co-precipitation method, Solar Energy 110 (2014) 386-397.
21. Humphreys R., Bimberg D., Choyke W., Wavelength modulated absorption in SiC, Solid State Comm. 39 (1981) 163-167.
22. Casady J., Johnson R., Status of silicon carbide (SiC) as a wide-bandgap semiconductor high-temperature applications: A review, Solid-State Electronics 39 (10 (1996) 1409-1422.
23. Yu B., Kwak S., Carbon quantum dots embedded with mesoporous hematite nanospheres as efficient visible light-active photocatalysts, J. Mater. Chem. 22 (2012) 8345-8353.

5. Conclusion

ZrC nanopowder were synthesized successfully by using single step carbo-thermal route using zirconium oxide as Zr source, Mg as reducing element and hexane as C source. Among all the samples, the sample synthesized at 700 ºC with a holding time of 5h (5ZrC700) produced single phase ZrC as revealed by matching the XRD peaks with the standard ICDD card (03-065-0332). Since the carbon content was observed so the synthesis temperature was raised to 800 ºC. But, the carbon content was still prominent with the least in 2.5h of holding time. However, lattice parameter 'a' in the sample 5ZrC800 (4.697 Å) showed the least deviation from the standard value (4.69 Å). Therefore, the sample 5ZrC800 was used to optimize the carbon content by considering different stoichiometric ratios. At the stoichiometric ratio of ZrC and C (1:1) single phase ZrC at 800 °C with 5h of holding time was obtained. It further confirms that C is able to fill the octahedral voids to form a stable configuration. Lattice parameter 'a' was also calculated using Bragg's law and average value obtained was 4.7 Å which is close to the standard value of 4.69 Å. The particle size was obtained by Scherrer method with the average particle size calculated to be ~10.5 nm. Williamson-Hall method was also used to calculate the particle size and the corresponding strain in the as-synthesized samples by making use of the Uniform Strain Model (USM). It was observed that, strain in the particles varies with the variation in the synthesis parameters which is further confirmed from the peak widths. The thermal analysis of the sample with 1:1 stoichiometry (5ZrC800 C0.22) showed that ZrC nano powders were stable upto 250 ºC after which it started to oxidize. With the further increase in temperature, the diffusion of oxygen in ZrC becomes large and at temperature range of ~530 ºC it gets converted to ZrO_2. However, the sample 5ZrC700 which comparatively had more C than the other sample showed a difference in TG pattern showing more weight loss. HRTEM analysis showed agglomerated particles confirming the formation of carbon engulfed ZrC nano particle. The optical studies of the synthesized samples 5ZrC700 and 5ZrC800 C0.22 showed a band gap of ~2.5 eV, calculated with the help of Tauc plot. This value of band gap falls under the category of wide band-gap semiconductors. Furthermore, photo catalytic activity of sample 5ZrC800 C0.22 was also studied showing a degradation of 80% of Methylene Blue (MB) dye in 5h when exposed to solar radiation.

6. Future scope

ZrC nanopowders can also be synthesized using different carbon sources where the synthesis parameters (time and temperature) can also be optimized. Being a potential candidate as catalyst, the electrocatalytic and photocatalytic behavior of nano ZrC can be studied for various HER, ORR, OER in acidic/basic medium and different photochemical reactions (mineralization of organic pollutants, photocatalytic H_2 production, photocatalytic fuel formation) respectively.